Doubly Coupled Nested Tensor Decompositions with Application to Multirelay Multicarrier MIMO Communication Networks

Danilo S Rocha, C. Alexandre R. Fernandes, Gérard Favier

Doubly Coupled Nested Tensor Decompositions with Application to Multirelay Multicarrier MIMO Communication Networks

Danilo S. Rocha[a], C. Alexandre R. Fernandes[b,*], Gérard Favier[c]

[a] *Federal Institute of Education, Science and Technology of Ceará, campus Horizonte, Brazil*
[b] *Federal University of Ceará, campus Sobral, Brazil*
[c] *I3S Laboratory, University of Côte d'Azur, CNRS, Sophia Antipolis, France*

Abstract

Coupled tensor decompositions have emerged as a promising approach to analyze large dimensional datasets in the context of signal processing applications. In this paper, a general concept of doubly coupled decomposition (DCD) for high-order tensors is first proposed, extending the idea of coupled decompositions to doubly coupled nested structures which result from the contraction of two sets of tensors, each set depending on a specific mode. Two new decompositions are defined, the so-called doubly coupled nested Tucker decomposition (DCNTD) and doubly coupled nested PARAFAC decomposition (DCNPD). Uniqueness of these DCDs is analyzed. In a second part, we show how these DCDs can be used to model multirelay multicarrier MIMO cooperative communication networks with two different tensor codings at the source and relay nodes. Exploiting the multilinear structure of the received signals and assuming the coding tensors are known at the destination, semi-blind closed-form receivers are developed for jointly estimating the channels and transmitted symbols. The proposed receivers use Khatri-Rao and Kronecker product factorization algorithms. Identifiability conditions for system parameter estimation and design of the tensor codes are also addressed. Monte Carlo simulation results illustrate the performance improvement of the proposed DCD-based systems over existing state-of-the-art ones.

Keywords: tensor decompositions, coupled decompositions, higher-order tensors, MIMO systems, multirelay communication systems.

1. Introduction

During the last two decades, multiple-input multiple-output (MIMO) wireless communication systems have been one of the main fields of application of tensor tools. This is due to the fact that tensors, also called multiway arrays, are well suited for representing and analyzing multidimensional and multimodal signals [1, 2, 3, 4], as encountered in

*Corresponding author
Email addresses: danilo.rocha@ifce.edu.br (Danilo S. Rocha), alexandrefernandes@ufc.br (C. Alexandre R. Fernandes), favier@i3s.unice.fr (Gérard Favier)

cooperative MIMO communication systems using multiple relays, whose objective is to achieve the optimal diversity-multiplexing tradeoff. Exploiting the multilinear structure of the recived signals allows to derive semi-blind receivers for jointly estimating the channels and information symbols, without use of pilot sequences.

High order tensors naturally offer the possibility of taking simultaneously into account several diversities like space, time, frequency, polarization and code diversities, which induces the multilinear structure of the data. Tensors can also be used for designing tensor codings like tensor space time (TST) and tensor space time frequency (TSTF) codings, proposed in [5] and [6], respectively. Tensor decompositions are particularly useful for modeling MIMO cooperative systems with relays, as it will be illustrated in the present paper..

The design of MIMO communication systems with tensor codings has given rise to several new tensor models like the PARATUCK-(N_1, N) [5], generalized PARATUCK [6, 7], nested PARAFAC [8, 9, 10], nested Tucker [11], and generalized nested PARAFAC [12] models. A review of semi-blind receivers for point-to-point and cooperative systems can be found in [13] and [14], respectively.

Nested models, originally proposed for fourth-order tensors, can be interpreted as structured tensor train decompositions (TTD) [15], whose wagons are second- or third-order tensors concatenated in forming two successive parallel factors (PARAFAC) [16] or Tucker [17] decompositions which share a matrix factor.

It is worth noting that the number of modalities of a data tensor can be increased either by increasing its order or by coupling it with tensor and/or matrix decompositions that share one or several modes. Such a coupling approach, called data fusion, allows to improve detection, interpretation, recognition and classification tasks by a joint analysis of several data sets.

Coupled models, like coupled matrix-matrix, matrix-tensor and tensor-tensor factorizations, denoted respectively CMMF, CMTF and CTTF, have been initially used in the context of data fusion [18], with applications in various areas, such as recommendation systems, data mining, bioinformatics, neuroimaging, and signal processing, among many others.

Historically, joint analysis of a collection of measurement matrices led to CMMF models for solving data fusion problems. With the use of data tensors, CMTF and CTTF models have emerged as powerful tools for modeling, analyzing and fusing data in various fields of application.

CMTF model was introduced in [19] by coupling a PARAFAC, also called a canonical polyadic decomposition (CPD), with a matrix factorization, and using the nonlinear conjugate gradient algorithm to estimate the parameters. This type of model was used in [20] to merge electroencephalogram (EEG) and functional magnetic resonance imaging (fMRI) data with the goal of analyzing brain activity. Such a CMTF model composed of an incomplete third-order CPD coupled with a matrix factorization in one mode, was also considered in [21] for missing data recovery in the

context of sensory data analysis and metabolomics, which aims to detect chemical substances in biological fluids.

Various algorithms have been proposed to efficiently estimate the parameters of coupled sparse MTF (CSMTF) models of large-scale data. See for instance [22] and [23] for fast and parallel methods, called Turbo-SMT and S^3CMTF, respectively.

CTTF models were presented in [24, 25] for coupled CPD and block term decomposition (BTD) models sharing one factor matrix, with applications in array signal processing [26], and for multidimensional harmonic retrieval (MHR) [27, 28]. Note that coupled models lead to more relaxed uniqueness conditions comparatively to the case of separate decompositions [24, 25, 27, 28]. For coupled structured models, i.e. structured data fusion, two classes of algorithms are proposed in [29], namely quasi-Newton and nonlinear least-squares methods. The case of partially coupled models is also considered in [30, 31, 32]. In [33], the constrained Cramér-Rao bound (CRRB) is established for evaluating the parameter estimation performance in the case of general partially coupled models.

A coupled sparse TTF (CSTTF) model was used for the imputation of missing data in a third-order data tensor, represented by means of two Tucker models with a low-rank constraint under the form of nuclear norm, in the context of high-resolution hyperspectral images [34].

The concept of double CTTF was introduced in [35] with CPD models, denoted DC-CPD, sharing only one factor matrix assumed to be of full column rank. This work was generalized in [36, 37] to DC-CPD models sharing factor matrices in the first two modes, for solving the joint blind source separation problem with second-order statistics, in the underdetermined case.

In [38, 39, 40], the authors have extended the coupling concept to Tucker decompositions for representing multirelay MIMO communication systems with TST and STF codings, respectively. These works introduce coupled models sharing common factors between various nested Tucker decompositions (NTD) [11]. Trains of coupled CP and Tucker decompositions are also considered in [41].

In this paper, a novel and more general concept of doubly coupled decomposition (DCD) for high-order tensors sharing common tensor factors via two distinct nested structures, is proposed. The term "doubly coupled" is used to denote that each individual tensor model shares factors in two distinct modes, some factors depending on one index, while another set of factors depends on another index, and no factor is common to all the decompositions. The proposed general framework can be extended to more complex coupling structures to provide DCD models from any tensor decomposition. Unlike the doubly coupled models in [36, 37], the proposed DCDs are based on two distinct nested structures obtained by contracting two sets of tensors, each set depending on a specific mode.

The new proposed decompositions generalize the concept of double coupling to sets of NTDs [11] and nested PARAFAC decompositions (NPDs) [8] for sixth-order tensors sharing more than one common matrix factor. The

corresponding DCDs are denoted by DCNTD and DCNPD, respectively. It is demonstrated that these DCD models are unique up to scalar ambiguities if the core tensors of the individual NTDs and NPDs are a priori known, as it will be the case of the application to MIMO communication systems addressed in this paper.

In a second part, it is shown that the new DCDs can be exploited to model multirelay multicarrier MIMO cooperative communication networks, using two different tensor codings at the source and relay nodes. In the first case, tensor space-time-frequency (TSTF) [6] and tensor space-time (TST) [5] codings are used, which leads to a DCNTD model for the received signals. In the second case, Khatri–Rao space-time-frequency (KRSTF) [8] and Khatri–Rao space-time (KRST) [42] codings, which can be viewed as simpler versions of TST and TSTF codings, respectively, are considered at the source and relays nodes. That leads to a DCNPD model for the received signals. These DCD models are exploited to develop semi-blind closed-form receivers allowing to jointly estimate channel state information (CSI) and transmitted symbols. The proposed receivers use Khatri-Rao and Kronecker product factorization algorithms. It is worth noting that, unlike the MIMO relay systems in [14, 43, 44], the channel estimation is performed without using a training sequence. Moreover, the design of the tensor codes is also addressed. In particular, a set of tensor codes based on the discrete Fourier transform (DFT) is presented to avoid noise amplification. Monte Carlo simulation results show the better performance of the proposed DCD-based systems over existing state-of-the-art ones.

The main contributions of the present work can be summarized with the following propositions: (i) a generic framework for defining DCDs; (ii) two new doubly coupled decompositions, namely the DCNTD and DCNPD models; (iii) an uniqueness analysis of these DCDs; (iv) the development of two cooperative MIMO OFDM multirelay systems using two different tensor codings which induce DCNTD and DCNPD models for the received signals; (v) semi-blind closed-form receivers for the proposed communication systems; (vi) a comparison of tensor codes; and (vii) Monte Carlo simulation results to illustrate the effectiveness of the proposed receivers.

The rest of the paper is organized as follows. In Section 2, a brief overview of nested tensor decompositions is first given. Then, we introduce a new formalism for DCDs, with the DCNTD and DCNPD models as particular cases. Uniqueness of these DCD models is addressed. In Section 3, these new tensor decompositions are used to model two cooperative MIMO multirelay multicarrier systems based on two different tensor codings. In Section 4, semi-blind closed-form receivers are presented, and identifiability conditions are derived for system parameter estimation. The design of the tensor codes is also considered. In Section 5, Monte Carlo simulation results are provided to illustrate the effectiveness of the proposed cooperative systems. Section 6 concludes the paper.

Notation. In Table 1, the notations used in the manuscript are presented. Let $\mathcal{A} \in \mathbb{C}^{I_1 \times I_2 \times \cdots \times I_N}$ be an Nth-order tensor. The third-order tensor $\mathcal{A}_{J_1 \cdots J_{N-2} \times J_{N-1} \times J_N}$ is a contracted form of $\mathcal{A}$ obtained by combining the first $(N-2)$ modes along the first dimension of the tensor, where $\{J_1, \cdots, J_N\}$ represents a permutation of $\{I_1, \cdots, I_N\}$. Moreover, the matrix

Table 1: Notations

Symbols	Description
$a \in \mathbb{C}$	Scalar
$\mathbf{a} \in \mathbb{C}^I$	Column vector
$\mathbf{A} \in \mathbb{C}^{I \times J}$	Matrix
$\mathcal{A} \in \mathbb{C}^{I_1 \times I_2 \times \cdots \times I_N}$	N-order tensor (array of order higher than two)
$a_{i_1,i_2,\cdots,i_N}$ or $[\mathcal{A}]_{i_1,i_2,\cdots,i_N}$	$(i_1, i_2, \cdots, i_N)$-th element of the tensor $\mathcal{A}$
$\mathbf{A}^T$, $\mathbf{A}^H$, $\mathbf{A}^\dagger$, and $r_{\mathbf{A}}$	Transpose, Hermitian transpose, Moore-Penrose pseudo-inverse and rank of $\mathbf{A}$
$\mathbf{A}_{I_1 \cdots I_{N-1} \times I_N}$ or $[\mathcal{A}]_{I_1 \cdots I_{N-1} \times I_N}$	Mode-N tall unfolding of $\mathcal{A}$ (matrix representation of $\mathcal{A}$ obtained by combining the first $(N-1)$ modes
$\mathbf{x}_{:jk}$, $\mathbf{x}_{i:k}$, and $\mathbf{x}_{ij:}$	Vector slices (row, column, and tube) of $\mathcal{X} \in \mathbb{C}^{I \times J \times K}$
$\mathbf{X}_{i::}$, $\mathbf{X}_{:j:}$, and $\mathbf{X}_{::k}$	Matrix slices of $\mathcal{X} \in \mathbb{C}^{I \times J \times K}$ of dimensions $J \times K$, $I \times K$ and $I \times J$, respectively
$\mathcal{A}_{(i_n)}$ or $\mathcal{A}_{\cdots i_n \cdots}$	Tensor slice of order $(N-1)$ obtained by fixing the n-th mode
$vec(\cdot)$	Vectorization operator
$diag(\cdot)$	Diagonal matrix built from the elements of the argument vector
$diag_n(\cdot)$	Diagonal matrix built from the elements of the n-th row of the argument matrix
$bdiag(\cdot)$	Block-diagonal operator ($bdiag(\mathbf{A}_k) \triangleq bdiag(\mathbf{A}_1, ..., \mathbf{A}_K)$)
$\circ$	Outer product
$\otimes$	Kronecker product
$\bowtie$	Block-Kronecker product
$\diamond$	Khatri-Rao product
$\times_n$	Mode-n product
$*_m^n$	Contraction operation

$\mathbf{A}_{I_1 \cdots I_{N-1} \times I_N}$ is the tall unfolding of $\mathcal{A}$ whose entries are $a_{i_1,\cdots,i_N} = \left[\mathbf{A}_{I_1 \cdots I_{N-1} \times I_N}\right]_{\bar{i},\, i_N}$, with $\bar{i} = (i_1 - 1)I_2 \cdots I_{N-1} + \cdots + (i_{N-2} - 1)I_{N-1} + i_{N-1}$. The mode-$n$ tall unfolding of $\mathcal{A}$, denoted by $\mathbf{A}_{I_1 \cdots I_{n-1} I_{n+1} \cdots I_N \times I_n}$, with $1 \leq n \leq N$, can be similarly defined.

The mode-n product of $\mathcal{A} \in \mathbb{C}^{I_1 \times \cdots \times I_N}$ by $\mathbf{U} \in \mathbb{C}^{P_n \times I_n}$, denoted by $\mathcal{X} = \mathcal{A} \times_n \mathbf{U} \in \mathbb{C}^{I_1 \times \cdots \times I_{n-1} \times P_n \times I_{n+1} \times \cdots \times I_N}$, yields an Nth-order tensor defined as $x_{i_1,\cdots,i_{n-1},p_n,i_{n+1},\cdots,i_N} = \sum_{i_n=1}^{I_n} a_{i_1,\cdots,i_n,\cdots,i_N} u_{p_n,i_n}$. Let $\mathcal{B} \in \mathbb{C}^{J_1 \times \cdots \times J_M}$ be an Mth-order tensor such that $I_n = J_m = K$. The contraction of $\mathcal{A}$ and $\mathcal{B}$ over their common mode, denoted by $\mathcal{Y} = \mathcal{A} *_n^m \mathcal{B} \in \mathbb{C}^{I_1 \times \cdots \times I_{n-1} \times J_1 \times \cdots \times J_{m-1} \times J_{m+1} \times \cdots \times J_M \times I_{n+1} \times \cdots \times I_N}$, yields the following $(N+M-2)$th-order tensor [45]: $y_{i_1,\cdots,i_{n-1},j_1,\cdots,j_{m-1},j_{m+1},\cdots,j_M,i_{n+1},\cdots,i_N} = \sum_{k=1}^{K} a_{i_1,\cdots,k,\cdots,i_N} b_{j_1,\cdots,k,\cdots,j_M}$. The block-Kronecker product is a Kronecker product of partitioned matrices. In the case of equally partitioned matrices, the block-Kronecker product is said to be balanced [46]. Let $\mathbf{A} = [\mathbf{A}_k] \in \mathbb{C}^{I \times KJ}$ and $\mathbf{B} = [\mathbf{B}_k] \in \mathbb{C}^{M \times KN}$ be partitioned matrices composed of K block-columns $\mathbf{A}_k \in \mathbb{C}^{I \times J}$ and $\mathbf{B}_k \in \mathbb{C}^{M \times N}$, respectively. The balanced block-Kronecker product is defined as $\mathbf{A} \bowtie \mathbf{B} = [\mathbf{A}_1 \otimes \mathbf{B}_1 \;\; \mathbf{A}_2 \otimes \mathbf{B}_2 \;\; \cdots \;\; \mathbf{A}_K \otimes \mathbf{B}_K] \in \mathbb{C}^{IM \times KJN}$.

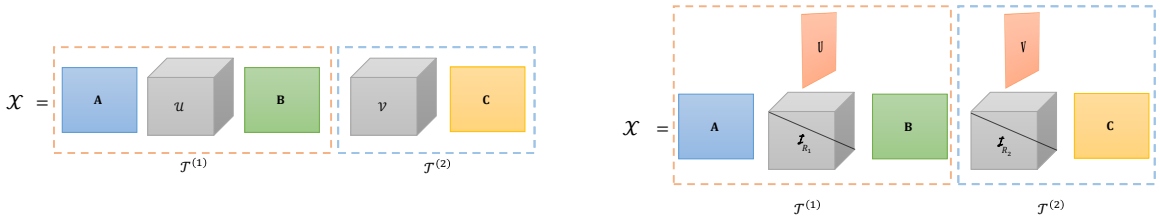

(a) (b)

Figure 1: Block-diagram of nested tensor decompositions: (a) NTD; (b) NPD.

The following properties will be used (matrices are assumed to be with compatible dimensions):

$$vec(\mathbf{ABC}^T) = (\mathbf{C} \otimes \mathbf{A})\, vec(\mathbf{B}), \tag{1}$$

$$vec(\mathbf{A}diag_n(\mathbf{B})\mathbf{C}^T) = (\mathbf{C} \diamond \mathbf{A})\, \mathbf{B}_{n\cdot}^T. \tag{2}$$

2. Tensor models

In this section, nested decompositions are first revisited and then coupled decompositions are briefly reviewed. At the end of this section, we present general doubly coupled tensor decompositions and propose two DCD models based on nested Tucker and nested PARAFAC decompositions.

2.1. Nested decompositions

The NTD and NPD, introduced respectively in [11] and [8], are recalled hereafter. Both models were originally introduced for a fourth-order tensor $\mathcal{X} \in \mathbb{C}^{I_1 \times I_2 \times I_3 \times I_4}$, as summarized in Table 2. Such nested models can be viewed as a cascade of two third-order Tucker or PARAFAC decompositions, which share the common matrix factor $\mathbf{B}$. They can also be written as the contraction (5) between two third-order tensors $\mathcal{T}^{(1)}$ and $\mathcal{T}^{(2)}$.

It is worth mentioning that the NPD can be viewed as a special case of the NTD when $R_1 = R_2$ and $R_3 = R_4$, and the core tensors $\mathcal{U}$ and $\mathcal{V}$ are respectively replaced by $\mathcal{I}_{R_1} \times_2 \mathbf{U}$ and $\mathcal{I}_{R_2} \times_2 \mathbf{V}$, where $\mathcal{I}_{R_1} \in \mathbb{C}^{R_1 \times R_1 \times R_1}$ and $\mathcal{I}_{R_2} \in \mathbb{C}^{R_2 \times R_2 \times R_2}$ are third-order identity tensors, i.e. diagonal tensors with ones on the main diagonal and zeros elsewhere. Equivalently, the NPD is obtained when the matrix slices $\mathbf{U}_{\cdot i_2 \cdot}$ and $\mathbf{V}_{\cdot i_3 \cdot}$ of the NTD are diagonal. The nested decompositions recalled in this subsection are depicted by block-diagrams in Fig. 1.

2.2. Coupled decompositions

Coupled tensor decompositions have emerged as important tools for analyzing multiple datasets in signal processing and statistics. A set of tensor decompositions is said to be "coupled" when at least one of the involved factors is

Table 2: Nested decompositions for $\mathcal{X} \in \mathbb{C}^{I_1 \times I_2 \times I_3 \times I_4}$

NTD	NPD
Scalar writing:	
$x_{i_1,i_2,i_3,i_4} = \sum_{r_1=1}^{R_1} \sum_{r_2=1}^{R_2} \sum_{r_3=1}^{R_3} \sum_{r_4=1}^{R_4} a_{i_1,r_1} u_{r_1,i_2,r_2} b_{r_2,r_3} v_{r_3,i_3,r_4} c_{i_4,r_4}$ (3)	$x_{i_1,i_2,i_3,i_4} = \sum_{r_1=1}^{R_1} \sum_{r_2=1}^{R_2} a_{i_1,r_1} u_{i_2,r_1} b_{r_1,r_2} v_{i_3,r_2} c_{i_4,r_2}$ (4)
Matrix and tensor factors:	
$\mathcal{U} \in \mathbb{C}^{R_1 \times I_2 \times R_2}$, $\mathcal{V} \in \mathbb{C}^{R_3 \times I_3 \times R_4}$, $\mathbf{A} \in \mathbb{C}^{I_1 \times R_1}$, $\mathbf{B} \in \mathbb{C}^{R_2 \times R_3}$, $\mathbf{C} \in \mathbb{C}^{I_4 \times R_4}$	$\mathbf{U} \in \mathbb{C}^{I_2 \times R_1}$, $\mathbf{V} \in \mathbb{C}^{I_3 \times R_2}$, $\mathbf{A} \in \mathbb{C}^{I_1 \times R_1}$, $\mathbf{B} \in \mathbb{C}^{R_1 \times R_2}$, $\mathbf{C} \in \mathbb{C}^{I_4 \times R_2}$
Writing as a tensor contraction:	
$\mathcal{X} = \mathcal{T}^{(1)} *_3^1 \mathcal{T}^{(2)}$ (5)	
Tensors $\mathcal{T}^{(1)}$ and $\mathcal{T}^{(2)}$:	
$t^{(1)}_{i_1,i_2,r_3} = \sum_{r_1=1}^{R_1} \sum_{r_2=1}^{R_2} a_{i_1,r_1} u_{r_1,i_2,r_2} b_{r_2,r_3}$ (6)	$t^{(1)}_{i_1,i_2,r_2} = \sum_{r_1=1}^{R_1} a_{i_1,r_1} u_{i_2,r_1} b_{r_1,r_2}$ (7)
$t^{(2)}_{r_3,i_3,i_4} = \sum_{r_4=1}^{R_4} v_{r_3,i_3,r_4} c_{i_4,r_4}$ (8)	$t^{(2)}_{r_2,i_3,i_4} = v_{i_3,r_2} c_{i_4,r_2}$ (9)

common to all the decompositions. The concept of coupled tensor decompositions was first applied to CPD models [35]. Recently, an extension of the coupling concept to Tucker decompositions was proposed in [38]. We now introduce two new coupled structures based on nested Tucker models.

The coupled nested Tucker decomposition (CNTD) can be viewed as a coupling of multiple NTDs that share a common factor [38]. Let $\mathcal{X}_{(k)} \in \mathbb{C}^{I_1 \times I_2 \times I_3 \times I_4}$, for $k = 1, ..., K$ and $K \geq 2$, be a tensor that satisfies a fourth-order NTD, as defined in (5), with the factor $\mathcal{T}^{(1)}$ depending on the index k, that is:

$$\mathcal{X}_{(k)} = \mathcal{T}^{(1)}_{(k)} *_3^1 \mathcal{T}^{(2)}, \tag{10}$$

where $\mathcal{T}^{(1)}_{(k)}$ is obtained by rewriting (6) as follows:

$$\mathcal{T}^{(1)}_{(k)} = \mathcal{U}_{(k)} \times_1 \mathbf{A}_{(k)} \times_3 \mathbf{B}^T_{(k)} \in \mathbb{C}^{I_1 \times I_2 \times R_3}. \tag{11}$$

The CNTD model represents a fifth-order tensor $\mathcal{X} \in \mathbb{C}^{I_1 \times I_2 \times I_3 \times I_4 \times K}$ composed of the tensors $\mathcal{X}_{(k)}$ that share the tensor $\mathcal{T}^{(2)}$, independent of the index k and common to all K decompositions. In a scalar notation, the CNTD of $\mathcal{X}_{(k)}$ is given by

$$x_{i_1,i_2,i_3,i_4,k} = \sum_{r_1=1}^{R_1} \sum_{r_2=1}^{R_2} \sum_{r_3=1}^{R_3} \sum_{r_4=1}^{R_4} a_{i_1,r_1,k} u_{r_1,i_2,r_2,k} b_{r_2,r_3,k} v_{r_3,i_3,r_4} c_{i_4,r_4}. \tag{12}$$

An alternative CNTD model was proposed in [39] by assuming a structure symmetric to the one presented in (10)-(12). From (5), let $\mathcal{X}_{(f)} \in \mathbb{C}^{I_1 \times I_2 \times I_3 \times I_4}$, for $f = 1, ..., F$ and $F \geq 2$, be a tensor that satisfies a fourth-order NTD,

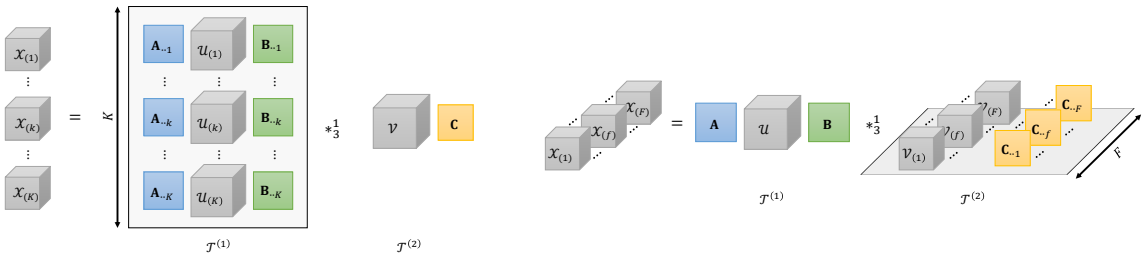

(a) (b)

Figure 2: Block-diagram of coupled nested Tucker decompositions: (a) Eqs. (10)-(11); (b) Eqs. (13)-(14).

with the factor $\mathcal{T}^{(2)}$ depending on the index f and $\mathcal{T}^{(1)}$ independent of f and common to all F decompositions. The CNTD (10) then becomes

$$\mathcal{X}_{(f)} = \mathcal{T}^{(1)} *_3^1 \mathcal{T}^{(2)}_{(f)}, \tag{13}$$

with

$$\mathcal{T}^{(2)}_{(f)} = \mathcal{V}_{(f)} \times_3 \mathbf{C}_{(f)} \in \mathbb{C}^{R_3 \times I_3 \times I_4}. \tag{14}$$

Figure 2 shows the block-diagram of these CNTDs, where the branches in each figure represent the collections of tensors $\{\mathcal{X}_{(1)}, \cdots, \mathcal{X}_{(K)}\}$ and $\{\mathcal{X}_{(1)}, \cdots, \mathcal{X}_{(F)}\}$ that form coupled NTDs sharing the common tensors $\mathcal{T}^{(2)}$ and $\mathcal{T}^{(1)}$, respectively. In this paper, the idea of coupled decompositions is extended to higher-order tensors, with doubly coupling, which can be viewed as a combination of the structures presented in (10) and (13).

2.3. Doubly coupled tensor decompositions (DCDs)

Following the coupled structures revisited in Subsection 2.2 and illustrated in Fig. 2, the main idea of a DCD is that some coupled factors depend on one index, while another set of coupled factors depends on another index, with no factor being common to all the decompositions.

For clarifying the general idea of DCD, let $\mathcal{X}$ be a tensor satisfying a decomposition with the tensor factors $\mathcal{A}^{(p)}_{(k)}$ and $\mathcal{B}^{(q)}_{(f)}$, for $p = 1, ..., P$ and $q = 1, ..., Q$, the set of factors $\{\mathcal{A}^{(1)}_{(k)}, \cdots, \mathcal{A}^{(P)}_{(k)}\}$ varying with the index $k = 1, ..., K$ and $\{\mathcal{B}^{(1)}_{(f)}, \cdots, \mathcal{B}^{(Q)}_{(f)}\}$ depending on the index $f = 1, ..., F$.

Thus, the tensor $\mathcal{X}$ depends on the indices (f, k), performing a double coupling. Indeed, if k is fixed, the tensor slice $\mathcal{X}_{(k)}$ follows a standard coupled decomposition, as well as the tensor slice $\mathcal{X}_{(f)}$, for some f fixed. If both k and f are fixed, the tensor slice $\mathcal{X}_{(f,k)}$ satisfies a non-coupled decomposition with $\{\mathcal{A}^{(1)}_{(k)}, \cdots, \mathcal{A}^{(P)}_{(k)}, \mathcal{B}^{(1)}_{(f)}, \cdots, \mathcal{B}^{(Q)}_{(f)}\}$ as factors. In what follows, DCD is detailed for the particular cases of NTDs and NPDs.

A. Proposed DCNTD and DCNPD

The proposed DCDs are based on the contraction operation between two tensors, similarly to the NTD and NPD expressed by means of Eq. (5). However, in the doubly coupled models, it is assumed that the tensor $\mathcal{X}$ is characterized by two indices (f, k), each one being associated with one coupling. The general structure of the proposed DCNTD and DCNPD for a sixth-order tensor is given by

$$\mathcal{X}_{(f,k)} = \mathcal{T}^{(1)}_{(k)} *_3^1 \mathcal{T}^{(2)}_{(f)} \in \mathbb{C}^{I_1 \times I_2 \times I_3 \times I_4}, \tag{15}$$

where $\mathcal{T}^{(1)}_{(k)} \in \mathbb{C}^{I_1 \times I_2 \times R_3}$ represents the tensor factor that depends on k, while $\mathcal{T}^{(2)}_{(f)} \in \mathbb{C}^{R_3 \times I_3 \times I_4}$ is the tensor factor depending on f. The DCNTD and DCNPD models represent a sixth-order tensor $\mathcal{X} \in \mathbb{C}^{I_1 \times I_2 \times I_3 \times I_4 \times F \times K}$ constructed by stacking the fourth-order tensor slices $X_{(f,k)}$ for $f = 1, ..., F$ and $k = 1, ..., K$, such as

$$\mathcal{X} = \mathcal{T}^{(1)} *_3^1 \mathcal{T}^{(2)}, \tag{16}$$

where $\mathcal{T}^{(1)} \in \mathbb{C}^{I_1 \times I_2 \times R_3 \times K}$ and $\mathcal{T}^{(2)} \in \mathbb{C}^{R_3 \times I_3 \times I_4 \times F}$ are the fourth-order tensors built from $\mathcal{T}^{(1)}_{(k)}$ and $\mathcal{T}^{(2)}_{(f)}$, respectively.

The difference between the DCNTD and DCNPD relies on the structure of the tensor factors $T^{(1)}_{(k)}$ and $\mathcal{T}^{(2)}_{(f)}$. For the DCNTD, these tensors have the structure defined by (6) and (8), as follows:

$$t^{(1)}_{i_1,i_2,r_3,k} = \sum_{r_1=1}^{R_1} \sum_{r_2=1}^{R_2} a_{i_1,r_1,k} u_{r_1,i_2,r_2,k} b_{r_2,r_3,k}, \qquad t^{(2)}_{r_3,i_3,i_4,f} = \sum_{r_4=1}^{R_4} v_{r_3,i_3,r_4,f} c_{i_4,r_4,f}, \tag{17}$$

which, for fixed k and f, correspond to Tucker-(2,3) and Tucker-(1,3) decompositions, respectively. For the DCNPD, the tensor factors $\mathcal{T}^{(1)}_{(k)}$ and $\mathcal{T}^{(2)}_{(f)}$ have the structure defined by (7) and (9), given by

$$t^{(1)}_{i_1,i_2,r_2,k} = \sum_{r_1=1}^{R_1} a_{i_1,r_1,k} u_{i_2,r_1,k} b_{r_1,r_2,k}, \qquad t^{(2)}_{r_2,i_3,i_4,f} = v_{i_3,r_2,f} c_{i_4,r_2,f}. \tag{18}$$

The proposed DCNTD and DCNPD can be respectively written in scalar form as follows:

$$x_{i_1,i_2,i_3,i_4,f,k} = \sum_{r_1=1}^{R_1} \sum_{r_2=1}^{R_2} \sum_{r_3=1}^{R_3} \sum_{r_4=1}^{R_4} a_{i_1,r_1,k} u_{r_1,i_2,r_2,k} b_{r_2,r_3,k} v_{r_3,i_3,r_4,f} c_{i_4,r_4,f}, \tag{19}$$

$$x_{i_1,i_2,i_3,i_4,f,k} = \sum_{r_1=1}^{R_1} \sum_{r_2=1}^{R_2} a_{i_1,r_1,k} u_{i_2,r_1,k} b_{r_1,r_2,k} v_{i_3,r_2,f} c_{i_4,r_2,f}. \tag{20}$$

These DCDs are useful to globally represent sets of NTDs and NPDs that share some common factors, by means

of a single higher-order tensor. Indeed, they allow a global processing of data sets, by exploiting the relationships between different groups of tensors. As it will be illustrated with simulation results for wireless communication networks, this approach allows an efficient and unified modeling of several communication systems, with a great flexibility on the choice of the system parameters.

B. Uniqueness

A tensor decomposition characterized by a contraction operation is generally not essentially unique. In [38], the authors showed that there are alternative solutions $\overline{\mathcal{T}}^{(1)}$ and $\overline{\mathcal{T}}^{(2)}$ that lead to the same contraction as $\mathcal{T}^{(1)}$ and $\mathcal{T}^{(2)}$, i.e. $\overline{\mathcal{T}}^{(1)} *_3^1 \overline{\mathcal{T}}^{(2)} = \mathcal{T}^{(1)} *_3^1 \mathcal{T}^{(2)}$. Hence, it is not possible to uniquely find the components $\mathcal{T}^{(1)}$ and $\mathcal{T}^{(2)}$ of a tensor defined by $\mathcal{X} = \mathcal{T}^{(1)} *_3^1 \mathcal{T}^{(2)}$. The proof of [38] is made for fifth-order tensors. However, it can be easily generalized to sixth-order tensors, as the DCDs considered in the present work.

Nevertheless, it was demonstrated in [38] that the contraction operation introduces scalar ambiguities only in the contracted modes. Indeed, it was shown that $\overline{\mathcal{T}}^{(2)}$ is characterized by an ambiguity matrix on the first mode, which corresponds to $\overline{\mathcal{T}}^{(2)} = \mathcal{T}^{(2)} \times_1 \mathbf{\Delta}^{-1}$. However, one can note from (17) and (18) that $\mathcal{T}^{(2)}$ contains only a mode-3 factor. Hence, it can be concluded that the mode-1 factor of $\mathcal{T}^{(2)}$ is equal to the identity matrix $\mathbf{I}_{R_3} \in \mathbb{C}^{R_3 \times R_3}$, which leads to $\mathbf{\Delta} = \delta \mathbf{I}_{R_3}$, with δ being a scalar ambiguity. The same result can be derived for the ambiguity of $\mathcal{T}^{(1)}$. This means that the tensors $\mathcal{T}^{(1)}$ and $\mathcal{T}^{(2)}$ are unique up to scalar ambiguities.

The issue that needs to be addressed now is whether the tensor factors $\mathcal{A} \in \mathbb{C}^{I_1 \times R_1 \times K}$ and $\mathcal{B} \in \mathbb{C}^{R_2 \times R_3 \times K}$ can be estimated from $\mathcal{T}^{(1)}$, as well as $\mathcal{C} \in \mathbb{C}^{I_4 \times R_4 \times F}$ from $\mathcal{T}^{(2)}$, when the core tensors $\mathcal{U}$ and $\mathcal{V}$ are assumed to be known, as it will be the case of the cooperative communication system considered in the next section. As is well known, the factor matrices of a Tucker decomposition are unique up to scalar ambiguities if the core tensor is known [11]. Hence, as the tensor factors $\mathcal{T}_{(k)}^{(1)}$ and $\mathcal{T}_{(f)}^{(2)}$ in a DCNTD model satisfy Tucker decompositions, the factors $\mathcal{A}$, $\mathcal{B}$, and $\mathcal{C}$ are unique up to scalar ambiguities when $\mathcal{U}$ and $\mathcal{V}$ are known.

Similarly, the essential uniqueness of the PARAFAC decomposition has been established under certain conditions [51, 53]. When one of the factor matrices is known, the other factors of a PARAFAC decomposition are unique up to scalar ambiguities in the columns of each matrix factor. Hence, as the factors $\mathcal{T}_{(k)}^{(1)}$ and $\mathcal{T}_{(f)}^{(2)}$ in a DCNPD model satisfy PARAFAC decompositions, $\mathcal{A} \in \mathbb{C}^{I_1 \times R_1 \times K}$, $\mathcal{B} \in \mathbb{C}^{R_1 \times R_2 \times K}$, and $\mathcal{C} \in \mathbb{C}^{I_4 \times R_2 \times F}$ are unique up to scalar ambiguities in their columns, when $\mathbf{U}$ and $\mathbf{V}$ are assumed to be known.

3. MIMO OFDM cooperative communication system

In this section, a new cooperative two-hop MIMO OFDM multirelay system based on DCD modeling is described. In Subsection 3.1.A, TSTF and TST codings are used at the source and relay nodes, respectively, leading to a DCNTD

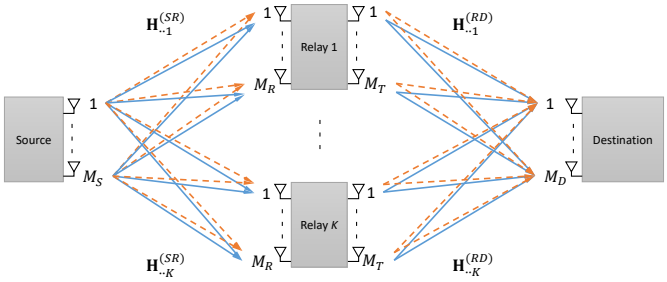

Figure 3: Cooperative two-hop MIMO OFDM multi-relay system.

model for the signals received at destination. In Subsection 3.1.B, KRSTF and KRST codings are considered at the source and relay nodes, respectively, which induces a DCNPD for the tensor of received signals. In Section 4, this DCD modeling is exploited to derive semi-blind closed-form receivers for jointly estimating the channels and information symbols.

3.1. System model

Let us consider the multicarrier two-hop MIMO multirelay system illustrated in Fig. 3, composed of one source (S), K relays ($R_1, \ldots, R_K$), and one destination (D). Different colored arrows represent the multiple subcarriers. The channels are assumed to be quasi-static frequency-flat fading, i.e. independent of the carrier frequency and invariant during the transmission. All the nodes of the system employ multiple antennas and the relays operate in half-duplex mode, with the amplify-and-forward (AF) protocol, meaning that the signals received at the relays are amplified and then forwarded to the destination node. In addition, the direct link between the source and destination node is assumed to be unavailable, corresponding to a link with deep fading.

It is also assumed that the relays are synchronized at symbol level, transmitting in orthogonal channels in different time slots. The global transmission is composed of $K + 1$ steps, the first step corresponding to the transmission from the source to the relays and the remaining K steps corresponding to the sequential transmission from the K relays to the destination. When a relay is transmitting to the destination, the other relays remain silent. Regarding the use of multiple relays operating in orthogonal channels, also known as parallel relaying, several works have used the same approach [43, 47, 14].

Table 3 gives the definitions and the dimensions of the tensors used for modeling the proposed system. The parameters that define the tensor dimensions are presented throughout the following subsections.

Table 3: System tensors and dimensions

	DCNTD-based system		DCNPD-based system	
Definitions	**Tensors**	**Dimensions**	**Tensors**	**Dimensions**
Symbols tensor	$\mathcal{S}$	$N \times R \times F$	$\mathcal{S}$	$N \times M_S \times F$
Source coding tensor	$\mathcal{C}^{(S)}$	$M_S \times P \times R \times F$	$\tilde{\mathcal{C}}^{(S)}$	$P \times M_S \times F$
Relay coding tensor	$\mathcal{C}^{(R)}$	$M_T \times J \times M_R \times K$	$\tilde{\mathcal{C}}^{(R)}$	$J \times M_T \times K$
SR channel tensor	$\mathcal{H}^{(SR)}$	$M_R \times M_S \times K$	$\mathcal{H}^{(SR)}$	$M_T \times M_S \times K$
RD channel tensor	$\mathcal{H}^{(RD)}$	$M_D \times M_T \times K$	$\mathcal{H}^{(RD)}$	$M_D \times M_T \times K$
Received signals tensor	$\mathcal{X}^{(D)}$	$M_D \times J \times P \times N \times F \times K$	$\mathcal{X}^{(D)}$	$M_D \times J \times P \times N \times F \times K$

A. DCNTD modeling

Let us assume that the source encodes the information signals to be transmitted, by means of a tensor space-time-frequency (TSTF) coding [6], while the relays use a tensor space-time (TST) coding [5]. The considered communication system can be viewed as a generalization of previous systems [11, 38, 39] by considering multiple relays and multiple carriers to send independent data. Combining multiple relays, multiple antennas and multiple carriers allows the exploitation of space and cooperative diversities, with multiplexing of transmitted symbols in space, time, and frequency domains.

In the sequel, for the sake of simplicity, the noiseless case is considered for describing the system model. The source node transmits the following TSTF coded data:

$$x^{(S)}_{m_S,p,n,f} = \sum_{r=1}^{R} c^{(S)}_{m_S,p,r,f} s_{n,r,f}, \tag{21}$$

where $x^{(S)}_{m_S,p,n,f}$ is the transmitted signal, $c^{(S)}_{m_S,p,r,f}$ is the TSTF code used by the source and $s_{n,r,f}$ is a data symbol, with $\mathcal{X}^{(S)} \in \mathbb{C}^{M_S \times P \times N \times F}$, $\mathcal{C}^{(S)} \in \mathbb{C}^{M_S \times P \times R \times F}$ and $\mathcal{S} \in \mathbb{C}^{N \times R \times F}$, M_S being the number of transmit antennas at the source node, P the time spreading length of the TSTF code, N the number of symbols per data stream, F the number of subcarriers used for transmission and R the number of data streams transmitted during each symbol period. Equation (21) shows that, for each subcarrier f, transmission block p, and symbol period n, the source transmits a linear combination of R data streams using the transmit antenna m_s. Note that each carrier sends independent data, which means that the data is multiplexed in the space, time, and frequency domains.

The signals are transmitted to K relays through the channels $\mathbf{H}^{(SR)}_{..k} \in \mathbb{C}^{M_R \times M_S}$ between the source and the relay k, for $k = 1, ..., K$, where M_R is the number of receive antennas at each relay. The subcarriers used by the source are assumed to be close enough so that the channel coefficients are invariant across the subcarriers. Due to this assumption, the number F of subcarriers cannot be very high. The signals received by the antenna m_R of relay k can

be expressed as

$$x^{(R)}_{m_R,p,n,f,k} = \sum_{m_S=1}^{M_S} h^{(SR)}_{m_R,m_S,k} x^{(S)}_{m_S,p,n,f} = \sum_{m_S=1}^{M_S} \sum_{r=1}^{R} h^{(SR)}_{m_R,m_S,k} c^{(S)}_{m_S,p,r,f} s_{n,r,f}, \tag{22}$$

where $\mathcal{H}^{(SR)} \in \mathbb{C}^{M_R \times M_S \times K}$ is the channel tensor that contains all the source-relay channel matrices. Each relay re-encodes the received signals using a TST coding before transmitting the re-encoded signals to the destination. The signals transmitted by antenna m_T of relay k are given by

$$x^{(T)}_{m_T,j,p,n,f,k} = \sum_{m_R=1}^{M_R} c^{(R)}_{m_T,j,m_R,k} x^{(R)}_{m_R,p,n,f,k} = \sum_{m_R=1}^{M_R} \sum_{m_S=1}^{M_S} \sum_{r=1}^{R} c^{(R)}_{m_T,j,m_R,k} h^{(SR)}_{m_R,m_S,k} c^{(S)}_{m_S,p,r,f} s_{n,r,f}, \tag{23}$$

where $\mathcal{C}^{(R)} \in \mathbb{C}^{M_T \times J \times M_R \times K}$ is the code tensor used at the relays, and J is the time spreading length of the TST code.

Finally, after transmission through the channel $\mathbf{H}^{(RD)}_{:,k} \in \mathbb{C}^{M_D \times M_T}$, for $k = 1, ..., K$, between the relay k and the destination, the signals received at destination are given by

$$x^{(D)}_{m_D,j,p,n,f,k} = \sum_{m_T=1}^{M_T} h^{(RD)}_{m_D,m_T,k} x^{(T)}_{m_T,j,p,n,f,k} = \sum_{m_T=1}^{M_T} \sum_{m_R=1}^{M_R} \sum_{m_S=1}^{M_S} \sum_{r=1}^{R} h^{(RD)}_{m_D,m_T,k} c^{(R)}_{m_T,j,m_R,k} h^{(SR)}_{m_R,m_S,k} c^{(S)}_{m_S,p,r,f} s_{n,r,f}, \tag{24}$$

where $\mathcal{X}^{(D)} \in \mathbb{C}^{M_D \times J \times P \times N \times F \times K}$, and $\mathcal{H}^{(RD)} \in \mathbb{C}^{M_D \times M_T \times K}$ is the tensor that contains all the relay-destination channel matrices. Equation (24) corresponds to the DCNTD given by (19), with the following correspondences:

$$(\mathcal{X}^{(D)}, \mathcal{H}^{(RD)}, \mathcal{C}^{(R)}, \mathcal{H}^{(SR)}, \mathcal{C}^{(S)}, \mathcal{S}) \quad \longleftrightarrow \quad (\mathcal{X}, \mathcal{A}, \mathcal{U}, \mathcal{B}, \mathcal{V}, \mathcal{C}) \tag{25}$$

$$(M_D, J, P, N, F, K, M_T, M_R, M_S, R) \quad \longleftrightarrow \quad (I_1, I_2, I_3, I_4, F, K, R_1, R_2, R_3, R_4). \tag{26}$$

Equation (24) can be rewritten as

$$x^{(D)}_{m_D,j,p,n,f,k} = \sum_{m_S=1}^{M_S} h^{(SRD)}_{m_D,j,m_S,k} x^{(S)}_{m_S,p,n,f}, \tag{27}$$

where $x^{(S)}_{m_S,p,n,f}$ is defined in (21), and the effective channel tensor between the source and the destination is defined as

$$h^{(SRD)}_{m_D,j,m_S,k} = \sum_{m_T=1}^{M_T} \sum_{m_R=1}^{M_R} h^{(RD)}_{m_D,m_T,k} c^{(R)}_{m_T,j,m_R,k} h^{(SR)}_{m_R,m_S,k}. \tag{28}$$

Equation (27) can be expressed as the following contraction between the effective channel tensor and the tensor of

coded signals transmitted by the source:

$$\mathcal{X}^{(D)} = \mathcal{H}^{(SRD)} *_3^1 \mathcal{X}^{(S)}, \tag{29}$$

with

$$\mathcal{X}^{(S)} = \mathcal{C}^{(S)} \times_3 \mathcal{S} \in \mathbb{C}^{M_S \times P \times N \times F}, \tag{30}$$

$$\mathcal{H}^{(SRD)} = \mathcal{C}^{(R)} \times_1 \mathcal{H}^{(RD)} \times_3 \mathcal{H}^{(SR)'} \in \mathbb{C}^{M_D \times J \times M_S \times K}, \tag{31}$$

where the tensor $\mathcal{H}^{(SR)'} \in \mathbb{C}^{M_S \times M_R \times K}$ is built by permuting the first two modes of $\mathcal{H}^{(SR)} \in \mathbb{C}^{M_R \times M_S \times K}$. From (29)-(31), we can conclude that the tensor $\mathcal{X}^{(D)}$ of received signals satisfies a DCNTD model (16), with $\mathcal{X}^{(S)}$ and $\mathcal{H}^{(SRD)}$ satisfying generalized Tucker-$(1, 4)$ and Tucker-$(2, 4)$ decompositions, respectively.

The double-coupling is associated with the indices f and k in (24) which represent the numbers of subcarriers and relays, respectively. In this case, the received signals tensor for fixed (f, k), satisfies a fourth-order NTD given by $\mathcal{X}_{(f,k)}^{(D)} = \mathcal{H}_{(k)}^{(SRD)} *_3^1 \mathcal{X}_{(f)}^{(S)} \in \mathbb{C}^{M_D \times J \times P \times N}$, where the factor $\mathcal{H}_{(k)}^{(SRD)}$ depends on the relay index k, common to all the subcarriers f, while the factor $X_{(f)}^{(S)}$ depends on the subcarrier f and is common to all the relays k, inducing the double coupling due to the use of multiple relays and multiple subcarriers.

Alternatively, by fixing only the index f, the received signals tensor satisfies a fifth-order CNTD: $\mathcal{X}_{(f)}^{(D)} = \mathcal{H}^{(SRD)} *_3^1 \mathcal{X}_{(f)}^{(S)} \in \mathbb{C}^{M_D \times J \times P \times N \times K}$. Similarly, if only the index k is fixed, we get the following CNTD: $\mathcal{X}_{(k)}^{(D)} = \mathcal{H}_{(k)}^{(SRD)} *_3^1 \mathcal{X}^{(S)} \in \mathbb{C}^{M_D \times J \times P \times N \times F}$. The tensors $\mathcal{X}_{(f)}^{(D)}$ and $\mathcal{X}_{(k)}^{(D)}$ represent couplings of K and F NTDs, respectively. Note that, for each subcarrier f, the tensor $\mathcal{X}_{(f)}^{(S)}$ is common to all relays and, for each relay k, the tensor $\mathcal{H}_{(k)}^{(SRD)}$ is common to all subcarriers. The double coupling exploits a global processing of the data in order to improve the estimation of unknown parameters, allowing performance gains in channel and symbol estimation simultaneously.

B. DCNPD modeling

A simpler model can be obtained by considering that each matrix slice of the tensor codes is diagonal, i.e. $\mathbf{C}_{(p,f)}^{(S)} \in \mathbb{C}^{M_S \times R}$ and $\mathbf{C}_{(j,k)}^{(R)} \in \mathbb{C}^{M_T \times M_R}$ are diagonal matrices, for $1 \leq p \leq P$, $1 \leq f \leq F$, $1 \leq j \leq J$, and $1 \leq k \leq K$. Note that these assumptions imply $M_S = R$ and $M_T = M_R$, respectively. These tensor codes are called KRSTF and KRST coding, respectively [8, 42]. The coding tensors are then defined as third-order tensors, in the following way: $\tilde{c}_{p,m_S,f}^{(S)} = c_{m_S,p,m_S,f}^{(S)}$ and $\tilde{c}_{j,m_T,k}^{(R)} = c_{m_T,j,m_T,k}^{(R)}$, with $\tilde{\mathcal{C}}^{(S)} \in \mathbb{C}^{P \times M_S \times F}$ and $\tilde{\mathcal{C}}^{(R)} \in \mathbb{C}^{J \times M_T \times K}$. The resulting communication network can be viewed as a generalization of the system in [8], which also uses a KRSTF coding, by considering multiple relays with different time spreadings at the source and the relay.

In this case, equation (24) of the signals received at the destination becomes

$$x^{(D)}_{m_D,j,p,n,f,k} = \sum_{m_T=1}^{M_T} \sum_{m_S=1}^{M_S} h^{(RD)}_{m_D,m_T,k} \tilde{c}^{(R)}_{j,m_T,k} h^{(SR)}_{m_T,m_S,k} \tilde{c}^{(S)}_{p,m_S,f} s_{n,m_S,f}, \tag{32}$$

which corresponds to the DCNPD model (20) with the following correspondences:

$$(\mathcal{X}^{(D)}, \mathcal{H}^{(RD)}, \tilde{\mathcal{C}}^{(R)}, \mathcal{H}^{(SR)}, \tilde{\mathcal{C}}^{(S)}, \mathcal{S}) \quad \longleftrightarrow \quad (\mathcal{X}, \mathcal{A}, \mathcal{U}, \mathcal{B}, \mathcal{V}, \mathcal{C}) \tag{33}$$

$$(M_D, J, P, N, F, K, M_T, M_S) \quad \longleftrightarrow \quad (I_1, I_2, I_3, I_4, F, K, R_1, R_2). \tag{34}$$

Equation (32) can be rewritten in scalar form as

$$x^{(D)}_{m_D,j,p,n,f,k} = \sum_{m_S=1}^{M_S} h^{(SRD)}_{m_D,j,m_S,k} x^{(S)}_{m_S,p,n,f}, \tag{35}$$

with

$$x^{(S)}_{m_S,p,n,f} = \tilde{c}^{(S)}_{p,m_S,f} s_{n,m_S,f}, \tag{36}$$

$$h^{(SRD)}_{m_D,j,m_S,k} = \sum_{m_T=1}^{M_T} h^{(RD)}_{m_D,m_T,k} \tilde{c}^{(R)}_{j,m_T,k} h^{(SR)}_{m_T,m_S,k}. \tag{37}$$

The tensor $\mathcal{X}^{(D)}$ can also be expressed using a contraction operation as in (29).

The double-coupling in (32) results from the indices f and k. In this case, the received signals form a fourth-order NPD given by $\mathcal{X}^{(D)}_{(f,k)} = \mathcal{H}^{(SRD)}_{(k)} *^1_3 \mathcal{X}^{(S)}_{(f)} \in \mathbb{C}^{M_D \times J \times P \times N}$. As well as for the DCNTD, the factor $\mathcal{H}^{(SRD)}_{(k)}$ is common to all the subcarriers f, while the factor $X^{(S)}_{(f)}$ is common to all the relays k. The spectral efficiency of the proposed multirelay system is proportional to $R/P(JK + 1)$, for both tensor codings.

4. Semi-blind receivers

Exploiting the DCD modeling of the received signals tensor allows to derive semi-blind closed-form receivers for jointly estimating the channels ($\mathcal{H}^{(RD)}$ and $\mathcal{H}^{(SR)}$) and symbol ($\mathcal{S}$) tensors, assuming that the coding tensors $\mathcal{C}^{(R)}$ and $\mathcal{C}^{(S)}$ are known at the destination, which ensures the uniqueness of the decompositions. For the DCNTD model, low-rank approximations based on the Kronecker product factorization (KPF) [48] and the block-Kronecker product factorization (BKPF) [49] are used, while for the DCNPD model a low-rank approximation based on the Khatri-Rao product factorization (KRPF) [50] is used. These low-rank approximations are based on rearrangements of the

Kronecker, block-Kronecker, and Khatri-Rao products into rank-one matrices, whose factors are estimated by means of the SVD algorithm.

4.1. DCNTD receiver

Let $\mathcal{X}^{(D)} \in \mathbb{C}^{M_D \times J \times P \times N \times F \times K}$ be the sixth-order tensor that satisfies a DCNTD, as defined in (24). Fixing the indices (p, f) and combining the first, second, and sixth modes give the following matrix unfolding of the tensor slice $\mathbf{X}^{(D)}_{\cdot\cdot p \cdot f \cdot}$ of $\mathcal{X}^{(D)}$, deduced from (27) and (21):

$$\begin{aligned}\left[\mathbf{X}^{(D)}_{\cdot\cdot p \cdot f \cdot}\right]_{JKM_D \times N} &= \mathbf{H}^{(SRD)}_{JKM_D \times M_S}\, \mathbf{X}^{(S)}_{\cdot p \cdot f} \\ &= \mathbf{H}^{(SRD)}_{JKM_D \times M_S}\, \mathbf{C}^{(S)}_{\cdot p \cdot f}\, \mathbf{S}^{T}_{\cdot\cdot f},\end{aligned} \tag{38}$$

where $\mathbf{C}^{(S)}_{\cdot p \cdot f} \in \mathbb{C}^{M_S \times R}$, $\mathbf{S}_{\cdot\cdot f} \in \mathbb{C}^{N \times R}$, and $\mathbf{H}^{(SRD)}_{JKM_D \times M_S}$ is a tall mode-3 unfolding of $\mathcal{H}^{(SRD)}$. Applying property (1) to (38), we obtain the vectorized form $\left[\mathbf{X}^{(D)}_{\cdot\cdot p \cdot f \cdot}\right]_{NJKM_D} = vec\left(\left[\mathbf{X}^{(D)}_{\cdot\cdot p \cdot f \cdot}\right]_{JKM_D \times N}\right)$ as follows:

$$\left[\mathbf{X}^{(D)}_{\cdot\cdot p \cdot f \cdot}\right]_{NJKM_D} = \left(\mathbf{S}_{\cdot\cdot f} \otimes \mathbf{H}^{(SRD)}_{JKM_D \times M_S}\right) vec\left(\mathbf{C}^{(S)}_{\cdot p \cdot f}\right). \tag{39}$$

Thus, the following tall matrix unfolding of $\mathcal{X}^{(D)}$ can be deduced:

$$\mathbf{X}^{(D)}_{NJKM_D \times FP} = \left(\mathbf{S}_{N \times FR} \otimes \mathbf{H}^{(SRD)}_{JKM_D \times M_S}\right) \mathbf{C}^{(S)}_{FRM_S \times FP}, \tag{40}$$

where $\mathbf{C}^{(S)}_{FRM_S \times FP} = bdiag\left[vec\left(\mathbf{C}^{(S)}_{\cdot 1 \cdot f}\right) \cdots vec\left(\mathbf{C}^{(S)}_{\cdot P \cdot f}\right)\right]$. The Kronecker product $\mathbf{\Omega} \triangleq \mathbf{S}_{N \times FR} \otimes \mathbf{H}^{(SRD)}_{JKM_D \times M_S} \in \mathbb{C}^{NJKM_D \times FRM_S}$ can be estimated from (40) using the least squares (LS) method as

$$\widehat{\mathbf{\Omega}} = \mathbf{X}^{(D)}_{NJKM_D \times FP} \left(\mathbf{C}^{(S)}_{FRM_S \times FP}\right)^{\dagger}. \tag{41}$$

Then, $\mathbf{S}_{N \times FR}$ and $\mathbf{H}^{(SRD)}_{JKM_D \times M_S}$ are estimated from the KPF estimate $\widehat{\mathbf{\Omega}}$ by applying the SVD-based low-rank approximation algorithm.

Once $\widehat{\mathbf{H}}^{(SRD)}_{JKM_D \times M_S}$ estimated, the channels $\mathcal{H}^{(RD)}$ and $\mathcal{H}^{(SR)}$ are estimated from the following reshaping $\widehat{\mathbf{H}}^{(SRD)}_{M_D M_S \times KJ}$ of $\widehat{\mathbf{H}}^{(SRD)}_{JKM_D \times M_S}$:

$$\widehat{\mathbf{H}}^{(SRD)}_{M_D M_S \times KJ} = \left(\mathbf{H}^{(RD)}_{M_D \times KM_T} \bowtie \mathbf{H}^{(SR)}_{M_S \times KM_R}\right) \mathbf{C}^{(R)}_{KM_T M_R \times KJ}, \tag{42}$$

where $\mathbf{C}^{(R)}_{KM_T M_R \times KJ} = bdiag\left[vec\left(\mathbf{C}^{(R)}_{\cdot 1 \cdot k}\right) \cdots vec\left(\mathbf{C}^{(R)}_{\cdot J \cdot k}\right)\right]$. The block-Kronecker product $\mathbf{\Psi} \triangleq \mathbf{H}^{(RD)}_{M_D \times KM_T} \bowtie \mathbf{H}^{(SR)}_{M_S \times KM_R} \in$

Algorithm 1 KPF/BKPF-based receiver for the DCNTD model

1. Build the unfolded matrix $\mathbf{X}^{(D)}_{NJKM_D\times FP}$.
2. Calculate the LS estimate $\widehat{\mathbf{\Omega}}$ using (41).
3. Estimate $\widehat{\mathbf{S}}_{N\times FR}$ and $\widehat{\mathbf{H}}^{(SRD)}_{JKM_D\times M_S}$ from $\widehat{\mathbf{\Omega}}$ using the SVD-based low-rank approximation for KPF.
4. Eliminate the ambiguities using (51).
5. Build $\widehat{\mathbf{H}}^{(SRD)}_{M_DM_S\times KJ}$ by reshaping $\widehat{\mathbf{H}}^{(SRD)}_{JKM_D\times M_S}$.
6. Calculate the LS estimate $\widehat{\mathbf{\Psi}}$ using (43).
7. Estimate $\widehat{\mathbf{H}}^{(RD)}_{M_D\times KM_T}$ and $\widehat{\mathbf{H}}^{(SR)}_{M_S\times KM_R}$ from $\widehat{\mathbf{\Psi}}$ using the SVD-based low-rank approximation for BKPF.
8. Eliminate the ambiguities using (52).

$\mathbb{C}^{M_DM_S\times KM_TM_R}$ is estimated from (42) using the LS method as follows:

$$\widehat{\mathbf{\Psi}} = \widehat{\mathbf{H}}^{(SRD)}_{M_DM_S\times KJ}\left(\mathbf{C}^{(R)}_{KM_TM_R\times KJ}\right)^{\dagger}. \tag{43}$$

Finally, by applying the low-rank approximation algorithm for BKPF, $\mathbf{H}^{(RD)}_{M_D\times KM_T}$ and $\mathbf{H}^{(SR)}_{M_S\times KM_R}$ are estimated from $\widehat{\mathbf{\Psi}}$. The proposed DCNTD receiver is summarized in Algorithm 1.

4.2. DCNPD receiver

Let $\mathcal{X}^{(D)} \in \mathbb{C}^{M_D\times J\times P\times N\times F\times K}$ be the sixth-order received signals tensor that satisfies a DCNPD, defined in (32). By fixing the indices p and f, the following matrix representation of $\mathcal{X}^{(D)}$ can be derived:

$$\begin{aligned}\left[\mathbf{X}^{(D)}_{\cdot\cdot p\cdot f\cdot}\right]_{JKM_D\times N} &= \mathbf{H}^{(SRD)}_{JKM_D\times M_S}\,\mathbf{X}^{(S)}_{\cdot p\cdot f}\\ &= \mathbf{H}^{(SRD)}_{JKM_D\times M_S}\,diag_p\left(\tilde{\mathbf{C}}^{(S)}_{\cdot\cdot f}\right)\mathbf{S}^{T}_{\cdot\cdot f},\end{aligned} \tag{44}$$

where $\mathbf{H}^{(SRD)}_{JKM_D\times M_S}$ is a tall mode-3 unfolding of $\mathcal{H}^{(SRD)} \in \mathbb{C}^{M_D\times J\times M_S\times K}$. Applying property (2) to (44) gives the following vectorized form $\left[\mathbf{X}^{(D)}_{\cdot\cdot p\cdot f\cdot}\right]_{NJKM_D} = vec\left(\left[\mathbf{X}^{(D)}_{\cdot\cdot p\cdot f\cdot}\right]_{JKM_D\times N}\right)$:

$$\left[\mathbf{X}^{(D)}_{\cdot\cdot p\cdot f\cdot}\right]_{NJKM_D} = \left(\mathbf{S}_{\cdot\cdot f}\diamond\mathbf{H}^{(SRD)}_{JKM_D\times M_S}\right)\tilde{\mathbf{C}}^{(S)}_{p\cdot f}. \tag{45}$$

By stacking these FP vectors $\left[\mathbf{X}^{(D)}_{\cdot\cdot p\cdot f\cdot}\right]_{NJKM_D}$, for $p = 1,...,P$ and $f = 1,...,F$, as block-columns, we obtain the following matrix unfolding of $\mathcal{X}^{(D)}$:

$$\mathbf{X}^{(D)}_{NJKM_D\times FP} = \left(\mathbf{S}_{N\times FM_S}\diamond\mathbf{\Phi}\right)\tilde{\mathbf{C}}^{(S)}_{FM_S\times FP}, \tag{46}$$

where $\tilde{\mathbf{C}}^{(S)}_{FM_S\times FP} = bdiag\left[\tilde{\mathbf{C}}^{(S)}_{1\cdot f}\ \cdots\ \tilde{\mathbf{C}}^{(S)}_{P\cdot f}\right]$ and $\mathbf{\Phi} = (\mathbf{1}^T_F\otimes\mathbf{H}^{(SRD)}_{JKM_D\times M_S}) \in \mathbb{C}^{JKM_D\times FM_S}$, with $\mathbf{1}_F \in \mathbb{R}^F$ being a column vector composed of ones. The Khatri-Rao product $\mathbf{\Omega} \triangleq \mathbf{S}_{N\times FM_S}\diamond\mathbf{\Phi} \in \mathbb{C}^{NJKM_D\times FM_S}$ can be estimated using the LS

Algorithm 2 KRPF-based receiver for the DCNPD model

1. Build the unfolded matrix $\mathbf{X}^{(D)}_{NJKM_D\times FP}$.
2. Calculate the LS estimate $\widehat{\mathbf{\Omega}}$ using (47).
3. Estimate $\widehat{\mathbf{S}}_{N\times FM_S}$ and $\mathbf{\Phi}$ from $\widehat{\mathbf{\Omega}}$ using the SVD-based low-rank approximation for KRPF.
4. Estimate $\widehat{\mathbf{H}}^{(SRD)}_{JKM_D\times M_S}$ from $\widehat{\mathbf{\Phi}}$ using the SVD-based low-rank approximation for KRPF.
5. Eliminate the ambiguities using (53).
6. Build $\widehat{\mathbf{H}}^{(SRD)}_{M_DM_S\times KJ}$ by reshaping $\widehat{\mathbf{H}}^{(SRD)}_{JKM_D\times M_S}$.
7. Calculate the LS estimate $\widehat{\mathbf{\Psi}}$ using (49).
8. Estimate $\widehat{\mathbf{H}}^{(RD)}_{M_D\times KM_T}$ and $\widehat{\mathbf{H}}^{(SR)}_{M_S\times KM_T}$ from $\widehat{\mathbf{\Psi}}$ using the SVD-based low-rank approximation for KRPF.
9. Eliminate the ambiguities using (53).

method as:

$$\widehat{\mathbf{\Omega}} = \mathbf{X}^{(D)}_{NJKM_D\times FP}\left(\tilde{\mathbf{C}}^{(S)}_{FM_S\times FP}\right)^{\dagger}, \tag{47}$$

and then, estimates of $\mathbf{S}_{N\times FM_S}$ and $\mathbf{\Phi}$ are obtained from $\widehat{\mathbf{\Omega}}$ by applying the SVD-based low-rank approximation KRPF algorithm. Noting that $\mathbf{\Phi}$ is composed of F repetitions of $\mathbf{H}^{(SRD)}_{JKM_D\times M_S}$, we can estimate $\mathbf{H}^{(SRD)}_{JKM_D\times M_S}$ by averaging the F blocks estimated from $\widehat{\mathbf{\Phi}}$. An alternative method to estimate $\mathbf{H}^{(SRD)}_{JKM_D\times M_S}$ consists in rewriting $\mathbf{\Phi}$ as the Khatri-Rao product $\mathbf{\Phi}^T = \mathbf{1}_{F\times JKM_D} \diamond (\mathbf{H}^{(SRD)}_{JKM_D\times M_S})^T$, where $\mathbf{1}_{F\times JKM_D} \in \mathbb{R}^{F\times JKM_D}$ is a matrix composed of ones, and then applying the KRPF algorithm to $\widehat{\mathbf{\Phi}}^T$. As the averaging method gives less good results, we omit this possibility in the following.

Once $\widehat{\mathbf{H}}^{(SRD)}_{JKM_D\times M_S}$ estimated, the factors $\widehat{\mathcal{H}}^{(RD)}$ and $\widehat{\mathcal{H}}^{(SR)}$ are estimated from the following reshaped unfolding $\widehat{\mathbf{H}}^{(SRD)}_{M_DM_S\times KJ}$:

$$\widehat{\mathbf{H}}^{(SRD)}_{M_DM_S\times KJ} = \left(\mathbf{H}^{(RD)}_{M_D\times KM_T} \diamond \mathbf{H}^{(SR)}_{M_S\times KM_T}\right)\tilde{\mathbf{C}}^{(R)}_{KM_T\times KJ}, \tag{48}$$

where $\tilde{\mathbf{C}}^{(R)}_{KM_T\times KJ} = bdiag\left[\tilde{\mathbf{C}}^{(R)}_{1\cdot k}\ \cdots\ \tilde{\mathbf{C}}^{(R)}_{J\cdot k}\right]$. The Khatri-Rao product $\mathbf{\Psi} \triangleq \mathbf{H}^{(RD)}_{M_D\times KM_T} \diamond \mathbf{H}^{(SR)}_{M_S\times KM_T} \in \mathbb{C}^{M_DM_S\times KM_T}$ is estimated using the LS method as:

$$\widehat{\mathbf{\Psi}} = \widehat{\mathbf{H}}^{(SRD)}_{M_DM_S\times KJ}\left(\tilde{\mathbf{C}}^{(R)}_{KM_T\times KJ}\right)^{\dagger}, \tag{49}$$

and then, once again $\widehat{\mathbf{H}}^{(RD)}_{M_D\times KM_S}$ and $\widehat{\mathbf{H}}^{(SR)}_{M_S\times KM_T}$ are obtained by applying the low-rank approximation algorithm for KRPF. The proposed DCNPD receiver is detailed in Algorithm 2.

4.3. Identifiability conditions and ambiguity removal

In this subsection, the identifiability conditions of the presented estimation algorithms are derived. Both algorithms use the SVD-based low-rank matrix approximation and LS estimation. The identifiability conditions result from the computation of the pseudo-inverses needed to estimate $\widehat{\mathbf{\Omega}}$ and $\widehat{\mathbf{\Psi}}$. This means that the unfoldings $\mathbf{C}^{(S)}_{FRM_S\times FP}$, $\mathbf{C}^{(R)}_{KM_TM_R\times KJ}$, $\tilde{\mathbf{C}}^{(S)}_{FM_S\times FP}$ and $\tilde{\mathbf{C}}^{(R)}_{KM_T\times KJ}$ in (41), (43), (47) and (49), respectively, must be full row rank. That induces the following necessary conditions: $P \geq M_SR$ and $J \geq M_TM_R$ for DCNTD, and $P \geq M_S$ and $J \geq M_T$ for DCNPD. Note that the proposed receiver for the DCNPD model has weaker constraints than the one for DCNTD.

The matrices estimated by the considered SVD-based low-rank approximation algorithms for KPF, BKPF, and KRPF are affected by scaling ambiguities, as discussed in Subsection 2.3.B, in the following way:

$$\widehat{\mathbf{A}} \otimes \widehat{\mathbf{B}} \longleftarrow (\mathbf{A}\delta) \otimes \left(\mathbf{B}\delta^{-1}\right), \quad \widehat{\mathbf{A}} \bowtie \widehat{\mathbf{B}} \longleftarrow \left[\mathbf{A}_1\delta_1 \otimes \mathbf{B}_1\delta_1^{-1} \ \cdots \ \mathbf{A}_K\delta_K \otimes \mathbf{B}_K\delta_K^{-1}\right], \quad \widehat{\mathbf{A}} \diamond \widehat{\mathbf{B}} \longleftarrow (\mathbf{A}\boldsymbol{\Delta}) \diamond \left(\mathbf{B}\boldsymbol{\Delta}^{-1}\right), \tag{50}$$

where δ and δ_k, with $k = 1, \ldots, K$, are scalar ambiguities and $\boldsymbol{\Delta}$ is a diagonal ambiguity matrix. These ambiguities are eliminated by applying the following relations:

$$\widehat{\mathbf{A}} \longleftarrow \delta^{-1}\,\widehat{\mathbf{A}} \qquad \text{and} \qquad \widehat{\mathbf{B}} \longleftarrow \delta\,\widehat{\mathbf{B}}, \tag{51}$$

$$\widehat{\mathbf{A}}_k \longleftarrow \delta_k^{-1}\,\widehat{\mathbf{A}}_k \qquad \text{and} \qquad \widehat{\mathbf{B}}_k \longleftarrow \delta_k\,\widehat{\mathbf{B}}_k, \tag{52}$$

$$\widehat{\mathbf{A}} \longleftarrow \widehat{\mathbf{A}}\,\boldsymbol{\Delta}^{-1} \qquad \text{and} \qquad \widehat{\mathbf{B}} \longleftarrow \widehat{\mathbf{B}}\,\boldsymbol{\Delta}. \tag{53}$$

To estimate the scalars δ and δ_k and the diagonal elements of the matrix $\boldsymbol{\Delta}$, some a priori knowledge in the matrices $\mathbf{A}$ or $\mathbf{B}$ is needed. This knowledge depends on the considered application. For the case addressed in this paper, one transmitted symbol ($s_{1,1,1}$) is assumed to be known, as well as one channel coefficient of each relay-destination link ($h^{(RD)}_{1,1,k}$), for $k = 1, ..., K$. In practice, this a priori information can be obtained simply by using one pilot-symbol sent from each relay to the destination. A similar procedure was adopted in other works [11, 47, 52, 53] in the context of relaying systems. For the DCNTD system, the ambiguity removal is implemented after Steps 3 and 7 of Algorithm 1, while for the DCNPD system, the ambiguity removal is carried out after Steps 3, 4, and 8 of Algorithm 2. The scalar ambiguity associated with Step 4 of Algorithm 2 can be estimated by exploiting the fact that one of the factors of this KPF is a matrix composed of ones.

4.4. Design of the coding tensors

To prevent noise amplification, we choose the tensor codes such that the following matrix unfoldings are DFT matrices: $\mathbf{C}^{(S)}_{FRM_S \times FP}$, $\mathbf{C}^{(R)}_{KM_TM_R \times KJ}$, $\tilde{\mathbf{C}}^{(S)}_{FM_R \times FP}$, and $\tilde{\mathbf{C}}^{(R)}_{KM_T \times KJ}$. That allows to simplify the computation of their pseudo-inverse in (41), (43), (47), and (49), respectively.

As these matrices have a block-diagonal structure, the blocks that form these matrices are chosen as truncated DFT matrices. Indeed, a block-diagonal matrix composed of unitary blocks is also a unitary matrix. For instance, we define the matrix $\mathbf{C}^{(S)}_{FRM_S \times FP}$ composed of F truncated DFT matrices of dimension $RM_S \times P$, each one being composed of the first RM_S rows of a DFT matrix of dimension $P \times P$, while $\mathbf{C}^{(R)}_{KM_TM_R \times KJ}$ is constructed from K truncated DFT matrices of dimension $M_TM_R \times J$, composed of the first M_TM_R rows of a DFT matrix of dimension $J \times J$. Similarly for $\tilde{\mathbf{C}}^{(S)}_{FM_R \times FP}$ and $\tilde{\mathbf{C}}^{(R)}_{KM_T \times KJ}$.

Table 4: Basic configuration used in the simulations

Description	Parameter	Value
Number of symbols per data stream	N	10
Number of data streams	R	2
Time-spreading length of the source coding	P	4
Time-spreading length of the relay coding	J	4
Number of subcarriers	F	4
Number of relays	K	2
Number of antennas at the source	M_S	2
Number of receiving antennas at the relay	M_R	2
Number of transmitting antennas at the relay	M_T	2
Number of antennas at the destination	M_D	2

With this proposed DFT-based coding, the pseudo-inverses in (41), (43), (47) and (49) can be replaced by Hermitian transposes. In the simulations, we compare this DFT-based coding with random tensor codes, whose elements have unit magnitude and phase randomly drawn from a uniform distribution between 0 and 2π. This coding will be called random coding.

In both kinds of tensor coding, the tensors are multiplied by scalar gains so that, in the noise-free case, all the nodes have the same transmission power and the total transmission power is kept constant and equal to 1, regardless of the number of relays and antennas. The tensors $\mathcal{C}^{(S)}$, $\mathcal{C}^{(R)}$, $\tilde{\mathcal{C}}^{(S)}$ and $\tilde{\mathcal{C}}^{(R)}$ are respectively multiplied by $\sqrt{P_N \,/\, (M_S\, R)}$, $\sqrt{P_N \,/\, (M_R\, M_T\, (P_N\, \sigma^2_{H_{SR}} + N_0))}$, $\sqrt{P_N \,/\, M_S}$ and $\sqrt{P_N \,/\, (\, M_T\, (\, P_N\, \sigma^2_{H_{SR}} + N_0))}$, where $\sigma^2_{H_{SR}}$ is the mean power of SR channels and $P_N = P_T/(K+1)$ is the transmission power of each transmission node.

5. Simulation results

In this section, the performance of the proposed DCD-based communication systems and their respective receivers is evaluated by means of Monte Carlo simulations, considering the two-hop OFDM MIMO multirelay system introduced in Section 3. The transmitted data symbols are independent identically distributed (i.i.d.) random variables drawn from a 4-QAM constellation. The channel tensors $\mathcal{H}^{(SR)}$ and $\mathcal{H}^{(RD)}$ are composed of i.i.d. entries, following a quasi-static Rayleigh fading, with an exponential path loss corresponding to an attenuation given by $1/d^4$, where $d = D/2$ is the distance of each hop, and D is the distance between the source and destination arbitrarily chosen equal to 1. The code tensors are generated as described in Subsection 4.4 and all the receive antennas are corrupted by additive white Gaussian noise (AWGN). Moreover, when not stated otherwise, the parameters shown in Table 4 are used.

The figures of merit used to evaluate the proposed receivers are the symbol error rate (SER) and the normalized mean square error (NMSE) of the SR and RD channels, averaged over 2×10^4 Monte Carlo runs and plotted as a function of the total transmission power P_T divided by the noise spectral density N_0, with P_T defined as the sum of

the transmission powers of all the transmitting antennas of the source and relays. The noise spectral density at the relays and the destination is assumed to be equal and, at each run, P_T is fixed and N_0 is calculated according to the desired P_T/N_0 value. The NMSE of the estimated channels is computed as follows:

$$\text{NMSE} = 10\log_{10}\left(\frac{1}{MC}\sum_{mc=1}^{MC}\frac{\|\mathcal{H}_{mc}-\widehat{\mathcal{H}}_{mc}\|_F^2}{\|\mathcal{H}_{mc}\|_F^2}\right), \tag{54}$$

with MC denoting the number of Monte Carlo runs. $\mathcal{H}_{mc}$ and $\widehat{\mathcal{H}}_{mc}$ represent respectively the simulated and estimated channel tensors at the mc-th Monte Carlo run.

5.1. Impact of tensor coding design and comparison with ZF receivers

The first simulations have the objective of evaluating the impact of the design of the coding tensors, by comparing the performance obtained with the DFT-based coding and the random coding, introduced in Subsection 4.4. Figure 4(a) shows the SER versus P_T/N_0 for the proposed DCNTD and DCNPD receivers, using these two tensor codings. It can be viewed from this figure that the DFT-based coding provides much smaller SERs than the random coding. As earlier explained, this is due to the fact that the DFT-based coding avoids the noise amplification that occurs when the random coding is used. For more details, see the discussion in Section 5 of [38].

Moreover, in order to have an upper bound for the performance of the proposed receivers, Fig. 4(a) also shows the SER obtained with the corresponding zero-forcing (ZF) receivers that assume perfect knowledge of all the channels. The ZF receivers for the DCNTD and for the DCNPD can be deduced from (40) and (46) respectively as:

$$\mathbf{S}_{FR\times N} = \left[\left(\mathbf{I}_{FP}\otimes\mathbf{H}^{(SRD)}_{JKM_D\times M_S}\right)\mathbf{C}^{(S)}_{FPM_S\times FR}\right]^{\dagger}\mathbf{X}^{(D)}_{FPJKM_D\times N}, \tag{55}$$

$$\mathbf{S}_{FM_S\times N} = \left[\left(\mathbf{I}_{FP}\otimes\mathbf{H}^{(SRD)}_{JKM_D\times M_S}\right)\tilde{\mathbf{C}}^{(S)}_{FPM_S\times FM_S}\right]^{\dagger}\mathbf{X}^{(D)}_{FPJKM_D\times N}. \tag{56}$$

These receivers are respectively denoted by DCNTD/ZF and DCNPD/ZF. The SER of the ZF receivers shown in Fig. 4(a) is obtained with the DFT-based coding. As expected, the DCNTD/ZF and DCNPD/ZF receivers provide smaller SERs than the respective DCNTD and DCNPD. The gap between the curves of the DCNTD and DCNTD/ZF, as well as the difference between the curves of the DCNPD and DCNPD/ZF, is approximately equal to 2.5 dB.

Moreover, this figure shows that the DCNTD outperforms the DCNPD, as well as the DCNTD/ZF performs better than the DCNPD/ZF, when the DFT-based coding is used. This is due to the fact that, with the DCNPD, the matrix slices of the tensor codes are diagonal, while in the DCNTD these matrix slices are full matrices, which makes the DCNTD more efficient in exploring more spatial diversity than the DCNPD.

However, when the random coding is used, the DCNPD performs better than the DCNTD, due to the noise ampli-

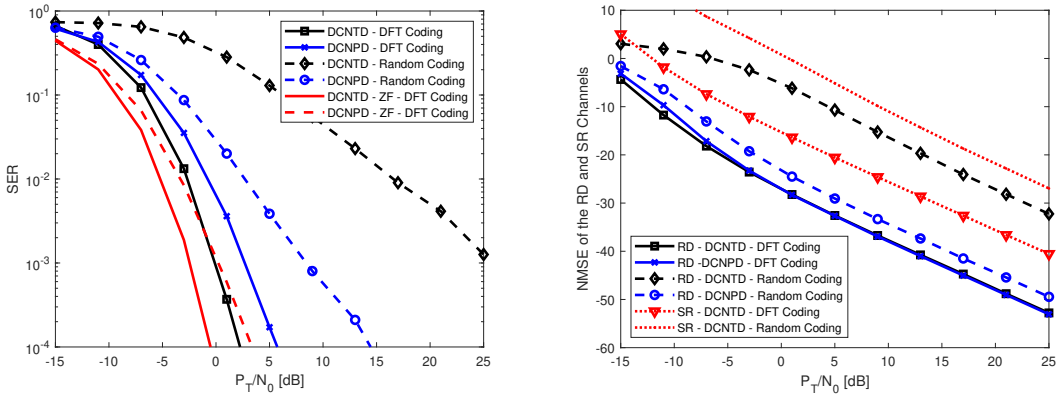

(a) (b)

Figure 4: Comparison of the DCNTD, DCNPD, DCNTD/ZF and DCNPD/ZF performance, using two tensor codings: (a) SER versus P_T/N_0; (b) NMSE versus P_T/N_0.

fication carried out by the random coding. In this case, the noise amplification is weaker with the DCNPD, due to the fact that the diagonal slices of the coding tensor to be inverted in (41), (43), (47), and (49) are better conditioned than in the case of the DCNTD.

Figure 4(b) shows the NMSE of the RD link versus P_T/N_0 for the proposed DCNTD and DCNPD receivers, using the two types of tensor codes. This figure also shows the NMSE of the SR link obtained by the DCNTD. From this figure, it can be concluded that, as expected, the DFT-based coding provides better NMSEs than the random coding, due to the noise amplification with random coding. Moreover, similarly as in Fig. 4(a), the DCNTD provides slightly better results than the DCNPD when the DFT-based coding is used, but worst results with random coding, due to the reasons above explained.

Besides, comparing the NMSEs of the SR and RD links obtained with the DCNTD, it can be concluded that the RD channels are better estimated than the SR channels. This is due to the fact that, as explained in Subsection 4.3, it is assumed that one channel coefficient of the RD link is known, while this assumption is not made for the SR link.

5.2. Influence of the number of relays, subcarriers, and antennas

The next figures evaluate the impact of the numbers (K, F, M) of relays, subcarriers, and antennas on the system performance. Due to the better performance of the DFT-based coding with respect to the random coding, from now on, all the simulation results are provided for the DFT-based coding. Figure 5(a) shows the SER versus P_T/N_0 for the proposed DCNTD and DCNPD receivers, for $K = 1$ relay and $K = 2$ relays. In these simulations, the length J of the time spreading at the relay, was adjusted so that the two tested cases have the same transmission rate, as indicated in the legend of Fig. 5(a). From this figure, it can be concluded that the use of 2 relays provides smaller SERs than

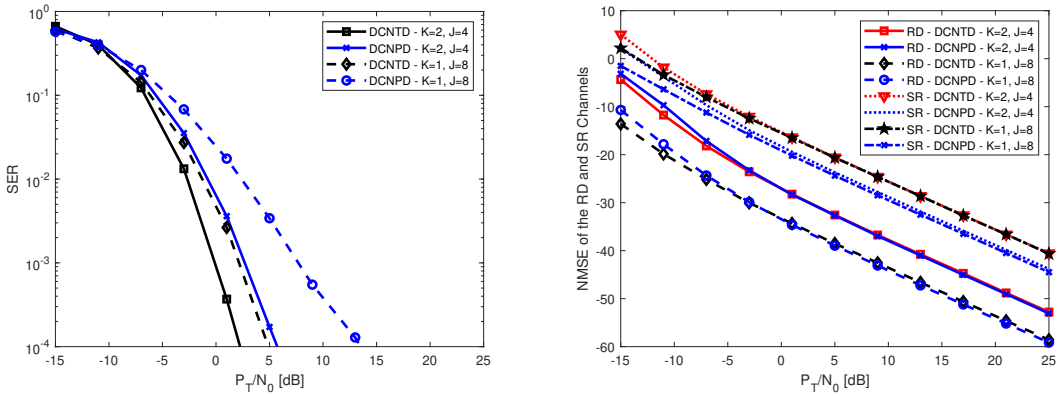

(a) (b)

Figure 5: Performance of the DCNTD and DCNPD for $K = 2, J = 4$ and $K = 1, J = 8$: (a) SER versus P_T/N_0; (b) NMSE versus P_T/N_0.

the case with a single relay. This is due to the cooperative diversity provided by the use of multiple relays. Moreover, as in Fig. 4(a), the DCNTD provides better SERs than the DCNTD, for the same reasons.

Fig. 5(b) shows the NMSE of the RD and SR links versus P_T/N_0 for the proposed DCNTD and DCNPD receivers, with the same configurations as Fig. 5(a), i.e. $K = 2$, $J = 4$ and $K = 1$, $J = 8$. From this figure, it can be viewed that the case $K = 1$, $J = 8$ provides smaller NMSEs than the case $K = 2$, $J = 4$. The reason is that the configuration $K = 2$, $J = 4$ has more channel coefficients to be estimated than the case $K = 1$, $J = 8$, for the same number of received signals. However, as expected, this worst behavior of the multirelay case with respect to the single-relay case, is due to the cooperative diversity which improves the symbol estimation, as viewed in Fig. 5(a), but degrades channel estimation.

Moreover, from Fig. 5(b), it can be drawn two conclusions that are similar to the ones for Fig. 4(b). The first conclusion is that the NMSE of the RD channels is smaller than the one of the SR channels. Besides, as in the previous results, the DCNTD provides slightly better channel estimations than the DCNPD.

Figures 6(a) and 6(b) show, respectively, the SER and NMSE of the RD link versus P_T/N_0 for several values of the number F of subcarriers, obtained with the proposed DCD receivers. The curves corresponding to the NMSE of the SR channels are similar to those of the RD channels and are omitted to alleviate the presentation. Moreover, the NMSE curves of the DCNPD are also omitted because they are very close to the ones of the DCNTD.

From Fig. 6(a), it can be viewed that, for both receivers, the SER does not change when the number of subcarriers is varied. That means, the proposed systems allow to increase the number of information symbols without degrading the SER performance due to a simultaneous increase of the number of received signals. Moreover, as in the previous SER results using the DFT-based coding, the DCNTD provides better SERs than the DCNPD. However, it can be

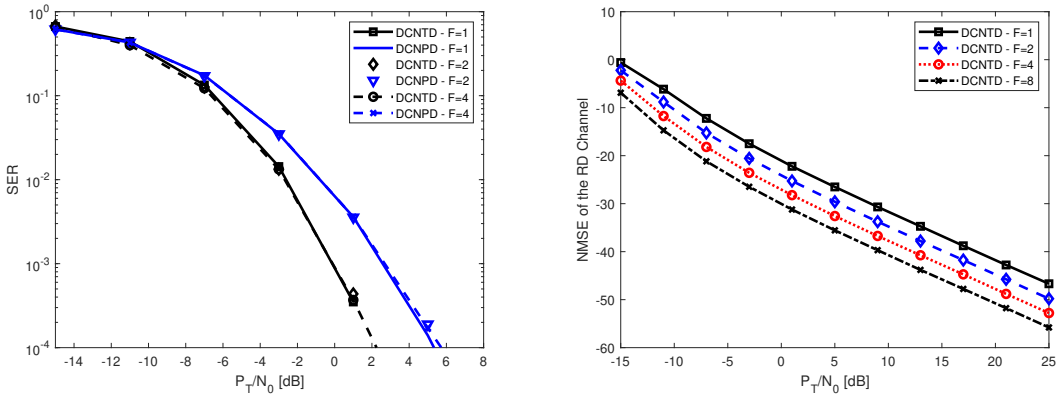

(a) (b)

Figure 6: Performance of the DCNTD and DCNPD for several values of F: (a) SER versus P_T/N_0; (b) NMSE of RD link versus P_T/N_0.

noted in Fig. 6(b) that the accuracy of the NMSE estimation is improved when the value of F is increased. These results show that exploiting more subcarriers in the DCD tensor model leads to a better channel estimation, without changing the SER and spectral efficiency.

Next figure evaluates the behavior of the symbol estimation when the number of antennas in all the nodes is varied. Figure 7 shows the SER versus P_T/N_0 with the DCNTD receiver, for several configurations of M_S, M_R, M_T and M_D. For all configurations, the values of M_S, M_R, M_T and M_D are equal to 2, except for one dimension equal to 4. It can be viewed from this figure that the best results are obtained when the number of receive antennas at the relay is increased ($M_R = 4$), while the other configurations provide roughly similar results. The reason for this behavior is twofold. The first one is that the spatial diversity at the receiver generally provides a higher array gain than the transmit spatial diversity. The second reason is that, when the number M_R of receive antennas at the relay is increased, the spatial diversity is induced in all the relays, leading to a more significant gain than increasing the number of antennas at the destination.

5.3. Comparison with state-of-the-art communication systems

In this subsection, we present simulation results that compare the proposed DCD-based systems with the following state-of-the-art tensor-based ones: (i) the single-carrier single-relaying MIMO system using TST coding proposed in [11], modeled as a NTD; (ii) the non-cooperative MIMO OFDM system using TSTF coding proposed in [39], modeled as a NTD; (iii) the single-carrier multirelay MIMO system using TST coding proposed in [38], modeled as a CNTD; (iv) the single-carrier single-relaying MIMO system using KRSTF coding proposed in [8], modeled as a NPD. These systems will be denoted respectively by NTD, NTD2, CNTD, and NPD.

The objective of these simulations is not to compare the efficiency of different estimation algorithms, but the

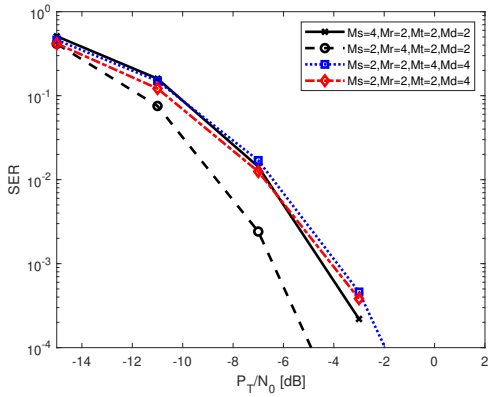

Figure 7: SER versus P_T/N_0 for the DCNTD for several values of M_S, M_R, M_T and M_D.

performance of different communication systems. Due to this, with all considered systems, we used receivers similar to those proposed in Section 4, with minor modifications in each case. Moreover, the parameters were set so that all the systems have the same spectral efficiency, using the following configurations: (i) for DCNTD and DCNPD - $F = 4, K = 2, J = 4, P = 4$; (ii) for NTD - $F = 1, K = 1, J = 8, P = 4$; (iii) for NTD2 - $F = 4, K = 1, J = 8, P = 4$; (iv) for CNTD - $F = 1, K = 2, J = 4, P = 4$; and (v) for NPD - $F = 1, K = 1, J = 8, P = 4$.

Figures 8(a) and 8(b) show, respectively, the SER and NMSE of the RD link versus P_T/N_0 for the compared systems. From these figures, it can be noted that the DCNTD and CNTD provide the best SER. This is due to the fact that these two systems, along with the DCNPD, use multiple relays and, therefore, benefit from cooperative diversity. Among these three systems that use multiple relaying, the DCNPD is the one that provides higher SERs, due to the fact that the matrix slices of the tensor code are diagonal, which makes it less efficient from the spatial diversity point of view, as already explained.

Even so, the SER obtained with the DCNPD is similar to the ones obtained with the Tucker-based models NTD and NTD2, and significantly smaller than the SER with the NPD, which also uses KRSTF coding. In fact, the NPD provides the highest SER among all the compared systems due to the use of diagonal matrix slices in the tensor code and to the fact that the NPD does not use multiple relays.

In Fig. 8(b), it can be viewed that DCNTD, DCNPD, NPD, and NTD provide similar NMSEs of the RD channels, while the NTD2 gives smaller NMSE. The better channel estimation of the NTD2 is due to the fact this system has less channel coefficients to be estimated than the other systems, as it is a non-cooperative system. On the other hand, the CNTD provides the highest NMSE among all the compared systems, due to the fact it uses multiple relays, therefore, with more channel coefficients to be estimated than the non-cooperative (NTD2) and single relay systems (NTD, NPD). It should be highlighted that, although the DCNTD and DCNPD also correspond to multi-relaying, their

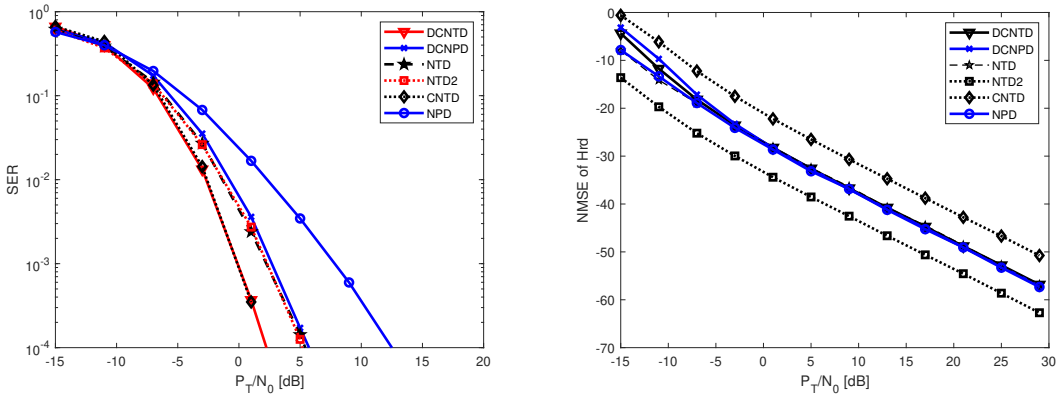

(a) (b)

Figure 8: Comparison of the DCNTD, DCNPD and state-of-the-art systems: (a) SER versus P_T/N_0; (b) NMSE of RD link versus P_T/N_0.

NMSE is similar to the single relay systems (NTD, NPD), which shows the efficiency of the proposed communication systems.

It can be concluded that the DCNTD is the method that offers the best trade-off between the SER and NMSE, as it provides the best SER, along with the CNTD, and the second best NMSE, along with the DCNPD, NPD, and NTD. Moreover, it is also worth noting that the PARAFAC-based DCNPD provides significantly better SER than the PARAFAC-based NPD, with similar NMSE results.

6. Conclusion

In the first part of the paper, we have introduced two new tensor decompositions for sixth-order tensors by exploiting the concepts of nested and doubly coupled decompositions (DCD). The so-called doubly coupled nested Tucker/PARAFAC decompositions, respectively denoted DCNTD and DCNPD, allow a global processing of high dimensional coupled data tensors. Uniqueness issue for these decompositions is addressed under the assumption of an a priori knowledge of the tensor cores, as it is the case of the proposed communication systems.

In a second part, a new multirelay multicarrier MIMO communication system has been proposed using either TST and TSTF codings, or KRST and KRSTF ones, at the source and relay nodes, which induces DCNTD and DCNPD models, respectively, for the tensors of signals received at the destination. Assuming DFT-based code tensors unfoldings for simplifying the computation, semi-blind closed-form receivers have been derived to jointly estimate the channels and transmitted symbols. Identifiability conditions of the proposed algorithms have been established. Monte Carlo simulation results illustrate the good performance of the proposed cooperative communication systems, providing a SER close to the one obtained with the ZF receiver that assumes a perfect knowledge of CSI.

From an analysis of the simulations results, it can be concluded that the proposed cooperative relaying systems provide a better tradeoff between SER and channel NMSE than state-of-the-art existing ones. These results corroborate the performance improvement of cooperative systems which exploit multiple relays, multiple subcarriers, with tensor codes. Moreover, the DCNTD-based system provides smaller SERs than PARAFAC-based systems, with similar channel NMSE. However, it is worth mentioning that the DCNPD-based system has less constraining identifiability conditions than the DCNTD-based one. In future works, the general framework proposed for nested DCD models will be extended to more complex coupling structures for designing new cooperative communications systems.

References

[1] A. Cichocki, D.P. Mandic, A.-H. Phan, C. Caiafa, G.-X. Zhou, Q.-B. Zhao, L. de Lathauwer, "Tensor decompositions for signal processing applications: From two-way to multiway component analysis", IEEE Signal Process. Mag., 32(2), 145-163, Mar. 2015.

[2] N.D. Sidiropoulos, L. de Lathauwer, X. Fu, K. Huang, E.E. Papalexakis, C. Faloutsos, "Tensor decomposition for signal processing and machine learning", IEEE Tr. Signal Process. 65(13), 3551-3582, 2017.

[3] G. Favier, "Matrix and Tensor Decompositions in Signal Processing", Wiley, USA, 2021.

[4] S. Miron, Y. Zniyed, R. Boyer, A.L.F. de Almeida, G. Favier, D. Brie, P. Comon, "Tensor methods for multisensor signal processing." *IET Signal Processing*, 14(10), 693-709, 2021.

[5] G. Favier, M.N. Costa, A.L.F. de Almeida, J.M.T. Romano, "Tensor space-time (TST) coding for MIMO wireless communication systems", *Signal Process.*, 92(4), 1079–1092, 2012.

[6] G. Favier, A.L.F. de Almeida, "Tensor space-time-frequency coding with semi blind receivers for MIMO wireless communication systems", *IEEE Trans. Signal Process.*, 62(22), 5987–6002, 2014.

[7] A.L.F. de Almeida, G. Favier, L.R. Ximenes, "Space-time-frequency (STF) MIMO communication systems With blind receiver based on a generalized PARATUCK2 model", IEEE Trans. Signal Process., 61(8), 1895-1909, 2013.

[8] A.L.F. de Almeida, G. Favier, "Double Khatri–Rao space-time-frequency coding using semi-blind PARAFAC based receiver", *IEEE Signal Process. Letters*, 20(5), 471–474, 2013.

[9] L.R. Ximenes, G. Favier, A.L.F. de Almeida, "Semi-blind receivers for non regenerative cooperative MIMO communications based on nested PARAFAC modeling", IEEE Tr. Signal Process. 63, 4985-4998, 2015.

[10] L.R. Ximenes, G. Favier, A.L.F. de Almeida, "Closed-form semi-blind receiver for MIMO relay systems using double Khatri-Rao space-time coding", IEEE Signal Process. Letters, 23(3), 316-320, Mar. 2016.

[11] G. Favier, C.A.R. Fernandes, A.L.F. de Almeida, "Nested Tucker tensor decomposition with application to MIMO relay systems using tensor space–time coding (TSTC)", *Signal Process.*, 128, 318–331, 2016.

[12] S.V.N. Randriambelonoro, G. Favier, R. Boyer, "Semi-blind joint symbols and multipath parameters estimation of MIMO systems using KRST/MKRSM coding", Digital Signal Process. 109, 102908, 2021.

[13] M.N. da Costa, G. Favier, J.M.T Romano, "Tensor modelling of MIMO communication systems with performance analysis and Kronecker receivers", Signal Process., 145(4), 304–316, 2018.

[14] C.A.R. Fernandes, A.L.F. de Almeida, D.B. Costa, "Unified tensor modeling for blind receivers in multiuser uplink cooperative systems", *IEEE Signal Process. Letters*., 19(5), 247–250, 2012.

[15] I. Oseledets, "Tensor-train decomposition", SIAM J. Sci. Computing, 33(5), 2295-2317, 2011.

[16] R. A. Harshman, "Foundations of the PARAFAC procedure: Model and conditions for an explanatory multimodal factor analysis", UCLA Working Papers in Phonetics, 16, 1-84, 1970.

[17] L.R. Tucker, Some mathematical notes on three-mode factor analysis, Psychometrika, 31, 279-311, 1966.

[18] D. Lahat, T. Adah, C. Jutten, "Multimodal data fusion: An overview of methods, challenges and prospects", Proceedings of the IEEE, 103(9), 1449-1477, 2015, hal-01179853.

[19] E. Acar, T.G. Kolda, D.M. Dunlavy, "All-at-once optimization for coupled matrix and tensor factorizations", in Proc. of Mining and Learning with Graphs, 2011, also in arXiv.org:1105.3422.

[20] E. Acar, Y. Levin-Schwartz, V.D. Calhoun, T. Adalı, "Tensor-based fusion of EEG and fMRI to understand neurological changes in schizophrenia", IEEE Int. Symp. on Circuits and Systems (ISCAS'2017), Baltimore, MD, USA, 2017, also in: arXiv: 1612.02189v1, 2016.

[21] E. Acar, M.A. Rasmussen, F. Savorani, T. Naes, R. Bro, Understanding data fusion within the framework of coupled matrix and tensor factorizations, Chemometrics and Intell. Lab. Syst., 129(15), 53-63, Nov. 2013.

[22] E.E. Papalexakis, T.M. Mitchell, N.D. Sidiropoulos, C. Faloutsos, P.P. Talukdar, B. Murphy, "Turbo-SMT: Accelerating coupled sparse matrix-tensor factorizations by 200x", in Proc. of SIAM Int. Conf. on Data Mining (SDM), 118-126, 2014.

[23] D. Choi, J.-G. Jang, U. Kang, "S^3CMTF: Fast, accurate, and scalable method for incomplete coupled matrix-tensor factorization", PLOS ONE, 14(6), June 2019.

[24] M. Sørensen, L. De Lathauwer, "Coupled canonical polyadic decompositions and (coupled) decompositions in multilinear rank-$(L_{r,n}, L_{r,n}, 1)$ terms – Part I: Uniqueness", SIAM J. Matrix Anal. Appl., 36(2), 496-522, 2015.

[25] M. Sorensen, I. Domanov, L. de Lathauwer, "Coupled canonical polyadic decompositions and (coupled) decompositions in multilinear rank-$(L_{r,n}, L_{r,n}, 1)$ terms - Part II: Algorithms", SIAM J. Matrix Anal. Appl., 36(3), 1015-1045, 2015.

[26] M. Sørensen, L. de Lathauwer, "Coupled tensor decompositions for applications in array signal processing." in *5th IEEE International Workshop on Computational Advances in Multi-Sensor Adaptive Processing (CAMSAP)*, Saint Martin, Dutch Antilles, 2013.

[27] M. Sørensen, L. de Lathauwer, "Multidimensional harmonic retrieval via coupled canonical polyadic decomposition - Part I: Model and identifiability, IEEE Tr. Signal Process., 65(2), 517-527, Jan. 2017.

[28] M. Sørensen, L. de Lathauwer, "Multidimensional harmonic retrieval via coupled canonical polyadic decomposition - Part II: Algorithm and multirate sampling, IEEE Tr. Signal Process., 65(2), 528-539, Jan. 2017.

[29] L. Sorber, M. Van Barel, L. de Lathauwer, "Structured data fusion", IEEE J. of Selected Topics in Signal Processing 9(4), 586-600, June 2015.

[30] R.C. Farias, J.E. Cohen, P. Comon, "Exploring multimodal data fusion through joint decompositions with flexible couplings, IEEE Tr. Signal Process., 64(18), 4830-4844, Sept. 2016.

[31] L. de Lathauwer, E. Kofidis, "Coupled matrix-tensor factorizations — The case of partially shared factors." Proc. of 51st Asilomar Conference on Signals, Systems, and Computers, IEEE, 2017.

[32] A.K. Smilde, I. Mage, T. Naes, T. Hankemeier, M.A. Lips, H.A.L. Kiers, E. Acar, R. Bro, Common and distinct components in data fusion, J. of Chemometrics, 31(7), e2900, 2017.

[33] C. Ren, R.C. Farias, P.-O. Amblard, P. Comon, "Performance bounds for coupled models", in IEEE Workshop on Sensor Array and Multichannel Signal Processing (SAM'2016), Rio de Janeiro, Brazil, Jul. 2016.

[34] S. Li, R. Dian, L. Fang, J.M. Bioucas-Dias, Fusing hyperspectral and multispectral images via coupled sparse tensor factorisation, IEEE Tr. on Image Processing, 27(8), 4118-4130, Aug. 2018.

[35] M. Sorensen, L. de Lathauwer, "Double coupled canonical polyadic decomposition with applications," *ESAT-STADIUS*, KU Leuven, Belgium,

Tech. Rep. 13–145, 2013.

[36] X.F. Gong, Q.H. Lin, F.Y. Cong, L. de Lathauwer, "Double coupled canonical polyadic decomposition for joint blind source separation," *IEEE Tr. Signal Processing*, 66(13), 3475-3490, 2018.

[37] X.F. Gong, Q.H. Lin, F.Y. Cong, L. de Lathauwer, "Double coupled canonical polyadic decomposition of third-order tensors: Algebraic algorithm and relaxed uniqueness conditions," *Signal Processing: Image Communication*, 73, 22-36, 2019.

[38] D.S. Rocha, C.A.R. Fernandes, G. Favier, "MIMO multi-relay systems with tensor space-time coding based on coupled nested Tucker decomposition", *Digital Signal Process.*, 89, 170-185, 2019.

[39] D.S. Rocha, C.A.R. Fernandes, G. Favier, "Space-Time-Frequency (STF) MIMO Relaying System with Receiver Based on Coupled Tensor Decompositions", in *52nd Asilomar Conference on Signals, Systems, and Computers*, Pacific Grove, CA, USA, pp. 328-332, 2018.

[40] D. S. Rocha, G. Favier, C. A. R. Fernandes, "Closed-form receiver for multi-hop MIMO relay systems with tensor space-time coding," *Journal of Communication and Information Systems*, 34(1), 50–54, 2019.

[41] Y. Zniyed, R. Boyer, A.L.F de Almeida, G. Favier, "High-order tensor estimation via trains of coupled third-order CP and Tucker decompositions," *Linear Algebra and its Applications*, 588, 304-337, 2020.

[42] N.D. Sidiropoulos, R.S. Budampati, "Khatri-Rao space-time codes", *IEEE Tr. Signal Process.*, 50(10), 2396-2407, 2002.

[43] Y. Rong, M.R.A. Khandaker, Y. Xiang, "Channel estimation of dual-hop MIMO relay system via parallel factor analysis", *IEEE Trans. Wireless Comm.*, 11, 2224–2233, 2012.

[44] C.W.R. Chiong, Y. Rong, Y. Xiang, "Channel training algorithms for two-way MIMO relay systems", IEEE Tr. Signal Process., 61(16), 3988-3998, 2013.

[45] A. Cichocki, "Tensor networks for big data analytics and large-scale optimization problems," *arXiv:1407.3124*, 2014.

[46] D.S. Tracy, "Balanced partitioned matrices and their Kronecker products," *Computational Statistics & Data Analysis*, 10(3), 315–323, 1990.

[47] X. Han, A.L.F. de Almeida, Z. Yang, "Channel estimation for MIMO multi-relay systems using a tensor approach", *EURASIP J. Adv. Signal Process.*, vol. 163, 2014.

[48] C.F. Van Loan, N. Pitsianis, "Approximation with Kronecker products," in *Moonen M.S., Golub G.H., De Moor B.L.R. (eds) Linear algebra for large scale and real-time applications*, Kluwer Academic Publishers, Netherlands, pp. 293–314, 1993.

[49] D.S. Rocha, "Nested tensor decomposition applied to cooperative MIMO communication systems," PhD thesis, Dept. Teleinformatics Eng., Federal University of Ceará, Fortaleza, Brazil, 2019.

[50] A.Y. Kibangou, G. Favier, "Non-iterative solution for PARAFAC with a Toeplitz matrix factor," in *17th European Signal Processing Conference*, pp. 691–695, 2009.

[51] N.D. Sidiropoulos, G.B. Giannakis, R. Bro. "Blind PARAFAC receivers for DS-CDMA systems," *IEEE Tr. Signal Processing*, 48(3), 810-823, 2000.

[52] J. Du, M. Han, Y. Hua, Y. Chen, H. Lin, "A robust semi-blind receiver for joint symbol and channel parameter estimation in multiple-antenna systems," *Electronics*, 8(5), 550, 2019.

[53] N.D. Sidiropoulos, R. Bro. "On the uniqueness of multilinear decomposition of N-way arrays", *J. of Chemometrics*, 14(3), 229-239, 2000.